JCI The Journal of Clinical Investigation

CD4+ follicular helper T cell infiltration predicts breast cancer survival

Chunyan Gu-Trantien, … , Christos Sotiriou, Karen Willard-Gallo

J Clin Invest. 2013;123(7):2873-2892. https://doi.org/10.1172/JCI67428.

Research Article Oncology

CD4+ T cells are critical regulators of immune responses, but their functional role in human breast cancer is relatively unknown. The goal of this study was to produce an image of CD4+ T cells infiltrating breast tumors using limited ex vivo manipulation to better understand the in vivo differences associated with patient prognosis. We performed comprehensive molecular profiling of infiltrating CD4+ T cells isolated from untreated invasive primary tumors and found that the infiltrating T cell subpopulations included follicular helper T (Tfh) cells, which have not previously been found in solid tumors, as well as Th1, Th2, and Th17 effector memory cells and Tregs. T cell signaling pathway alterations included a mixture of activation and suppression characterized by restricted cytokine/chemokine production, which inversely paralleled lymphoid infiltration levels and could be reproduced in activated donor CD4+ T cells treated with primary tumor supernatant. A comparison of extensively versus minimally infiltrated tumors showed that CXCL13-producing CD4+ Tfh cells distinguish extensive immune infiltrates, principally located in tertiary lymphoid structure germinal centers. An 8-gene Tfh signature, signifying organized antitumor immunity, robustly predicted survival or preoperative response to chemotherapy. Our identification of CD4+ Tfh cells in breast cancer suggests that they are an important immune element whose presence in the tumor is a prognostic factor.

CD4+ follicular helper T cell infiltration predicts breast cancer survival

Chunyan Gu-Trantien,[1] Sherene Loi,[2] Soizic Garaud,[1] Carole Equeter,[1,2] Myriam Libin,[1] Alexandre de Wind,[3] Marie Ravoet,[1] Hélène Le Buanec,[1] Catherine Sibille,[1] Germain Manfouo-Foutsop,[1] Isabelle Veys,[4] Benjamin Haibe-Kains,[2,5] Sandeep K. Singhal,[2] Stefan Michiels,[2] Françoise Rothé,[2] Roberto Salgado,[3] Hugues Duvillier,[1] Michail Ignatiadis,[2] Christine Desmedt,[2] Dominique Bron,[6] Denis Larsimont,[3] Martine Piccart,[7] Christos Sotiriou,[2] and Karen Willard-Gallo[1]

[1]Molecular Immunology Unit, [2]Breast Cancer Translational Research Laboratory JC Heuson, [3]Anatomical Pathology, and [4]Department of Surgery, Institut Jules Bordet, Université Libre de Bruxelles, Brussels, Belgium. [5]Computer Science, Université Libre de Bruxelles, Brussels, Belgium. [6]Department of Hematology and [7]Department of Medical Oncology, Institut Jules Bordet, Université Libre de Bruxelles, Brussels, Belgium.

CD4+ T cells are critical regulators of immune responses, but their functional role in human breast cancer is relatively unknown. The goal of this study was to produce an image of CD4+ T cells infiltrating breast tumors using limited ex vivo manipulation to better understand the in vivo differences associated with patient prognosis. We performed comprehensive molecular profiling of infiltrating CD4+ T cells isolated from untreated invasive primary tumors and found that the infiltrating T cell subpopulations included follicular helper T (Tfh) cells, which have not previously been found in solid tumors, as well as Th1, Th2, and Th17 effector memory cells and Tregs. T cell signaling pathway alterations included a mixture of activation and suppression characterized by restricted cytokine/chemokine production, which inversely paralleled lymphoid infiltration levels and could be reproduced in activated donor CD4+ T cells treated with primary tumor supernatant. A comparison of extensively versus minimally infiltrated tumors showed that CXCL13-producing CD4+ Tfh cells distinguish extensive immune infiltrates, principally located in tertiary lymphoid structure germinal centers. An 8-gene Tfh signature, signifying organized antitumor immunity, robustly predicted survival or preoperative response to chemotherapy. Our identification of CD4+ Tfh cells in breast cancer suggests that they are an important immune element whose presence in the tumor is a prognostic factor.

Introduction

Breast cancer (BC) is a complex and heterogeneous disease whose classification has been significantly improved in recent years through the development of gene expression signatures that currently identify 4 clinically distinct neoplastic diseases: luminal A and B, ER−, and HER2+ (1, 2). However, significant disparity in clinical outcome still remains within each of these disease entities, leading investigators to continue searching for more refinement. Initially, prognostic molecular signatures focused on the malignant cell, improving BC taxonomy via the assessment of genes regulating the cell cycle and proliferation (3, 4). More recently, attention has turned to the various nonneoplastic cells present in tumors, including stromal cells and infiltrating leukocytes, whose interactions with tumor cells can have a major influence on an individual patient's long-term outcome. Clinical studies using prognostic and predictive signatures have shown that the strength of the immune signal emanating from whole tumor gene expression profiles reflects the level of immune infiltration. A high immune signal has been linked with improved patient outcome in a variety of cancers (5), including subtypes of BC, with the strongest correlation for the latter observed in the ER− and HER2+ subtypes (6–13). Although there is not a consensus on the individual immune cell subset(s) that consistently mediates this effect, an important link between preexisting antitumor immune responses and long-term positive clinical outcome has been established (14).

Traditionally, CD8+ cytotoxic T cells have been considered as the key component of effective antitumor immunity, and breast tumors with higher levels of infiltrating CD8+ T cells have been associated with better patient survival (15, 16). However, studies have also shown that CD8+ T cells frequently fail to fully function in vivo if there is a lack of adequate CD4+ T cell help (17, 18). As central players in the immune system, CD4+ T cells perform critical roles in recruiting, activating, and regulating many facets of the adaptive immune response, with their helper functions for B cell– and CD8+ cytotoxic T cell–mediated responses well documented. CD4+ T cells also influence innate immunity by helping to shape the character and magnitude of the inflammatory response.

One common observation from functional studies is that many of the infiltrating leukocyte subpopulations do not expand or function normally within the tumor microenvironment. The current consensus is that IFN-γ–producing CD4+ Th1 and CD8+ T cells, along with mature DCs, NK cells, M1 macrophages, and type 1 NKT cells can generate effective although frequently attenuated antitumor responses, while CD4+ Th2 cells and type 2 NKT cells in cooperation with CD4+ Tregs (regulatory), myeloid-derived suppressor cells, immature DCs, or M2 macrophages suppress antitumor immunity and can also promote tumor progression (19–21). However, this generalization comes with the caveat that variation exists among tumor types, with the so-called protumorigenic cells, such as CD4+ Th17, also shown to produce effective antitumor responses (20, 22, 23). Emerging from these studies is recognition that the various CD4+ Th subsets have important functions in both protumor and antitumor immunity, with IFN-γ–producing

Conflict of interest: The authors have declared that no conflict of interest exists.
Citation for this article: *J Clin Invest.* 2013;123(7):2873–2892. doi:10.1172/JCI67428.

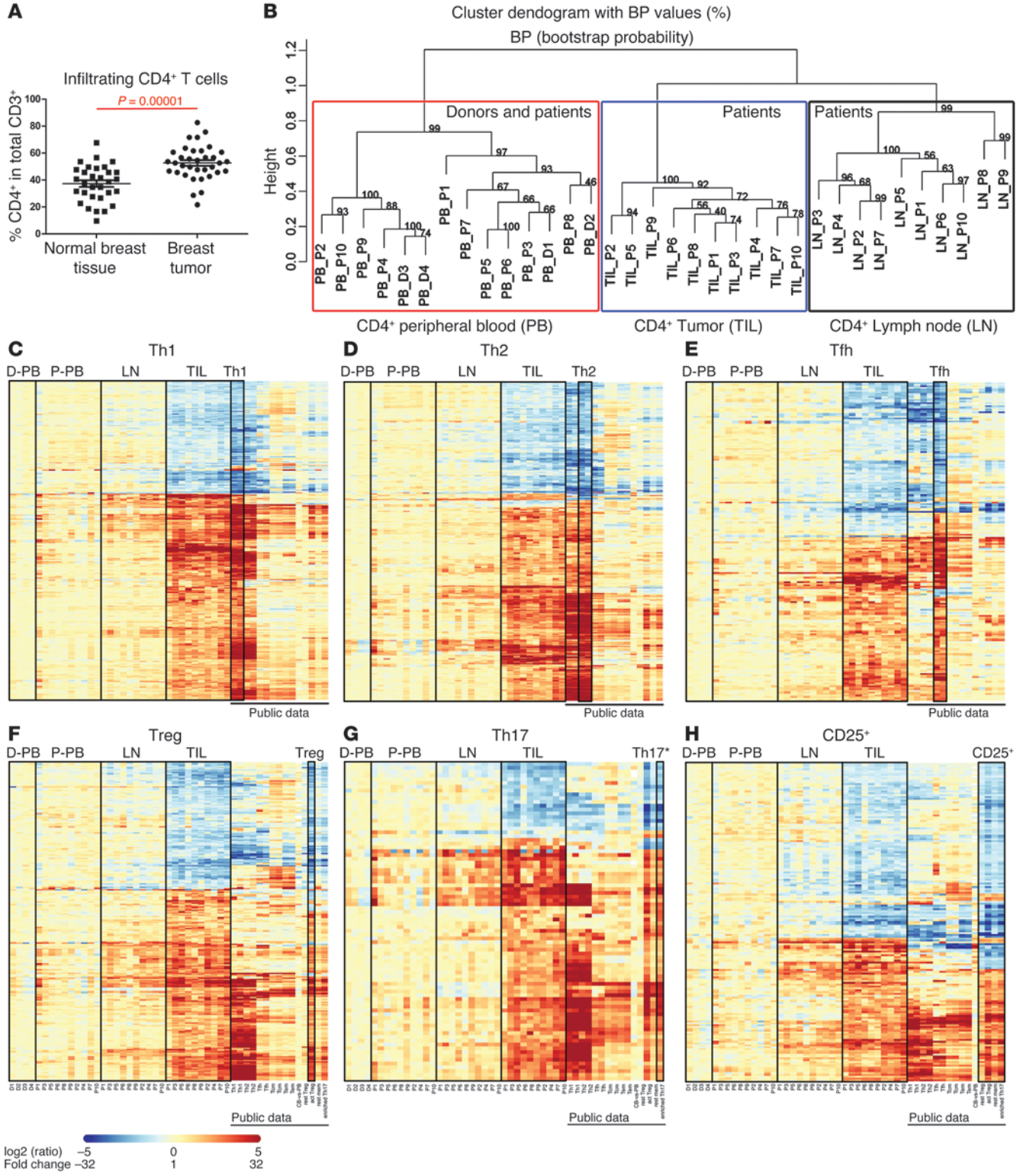
A
Infiltrating CD4+ T cells
P = 0.00001
% CD4+ in total CD3+
Normal breast tissue
Breast tumor
B
Cluster dendogram with BP values (%)
BP (bootstrap probability)
Height
Donors and patients
Patients
Patients
PB_P2
PB_P10
PB_P9
PB_P4
PB_D3
PB_D4
PB_P1
PB_P7
PB_P5
PB_P6
PB_P3
PB_D1
PB_P8
PB_D2
TIL_P2
TIL_P5
TIL_P9
TIL_P6
TIL_P8
TIL_P1
TIL_P3
TIL_P4
TIL_P7
TIL_P10
LN_P3
LN_P4
LN_P2
LN_P7
LN_P5
LN_P1
LN_P6
LN_P10
LN_P8
LN_P9
CD4+ peripheral blood (PB)
CD4+ Tumor (TIL)
CD4+ Lymph node (LN)
C
Th1
D-PB P-PB LN TIL Th1
Public data
D
Th2
D-PB P-PB LN TIL Th2
Public data
E
Tfh
D-PB P-PB LN TIL Tfh
Public data
F
Treg
D-PB P-PB LN TIL Treg
Public data
G
Th17
D-PB P-PB LN TIL Th17*
Public data
H
CD25+
D-PB P-PB LN TIL CD25+
Public data
log2 (ratio) −5 0 5
Fold change −32 1 32

Figure 1
Characteristics of CD4+ T cells infiltrating breast tumors. (**A**) The percentage of CD4+ within the CD3+ subpopulation was determined by flow cytometry (see Supplemental Figure 1). (**B**–**H**) Purified CD4+ T cells were from fresh tumor homogenates (TIL), LNs, P-PB, or D-PB (patient discovery set; Supplemental Table 1B). (**B**) Dendrogram of unsupervised hierarchical clustering analysis generated with pvclust using the top 5% (*n* = 2,734) most variable probe sets across all samples. Robustness was estimated by bootstrap analysis with the corresponding probability values (BP) shown. (**C**–**H**) Statistically significant gene changes established for the comparison of TIL versus P-PB (Supplemental Table 2B) were compared with public microarray data sets of human Th subpopulations that we reanalyzed (Supplemental Methods) to determine preferentially altered Th subset genes (Supplemental Table 3). Individual heat maps (red, upregulated; blue, downregulated) show genes altered in both the TIL and the indicated Th subset. Samples include our data (normalized to D1–D4 PB), D-PB (*n* = 4), P-PB (*n* = 10), LN (*n* = 10), TIL (*n* = 10), and public microarray data (normalized to naive cells in the same data set), Th1 (*n* = 2), Th2 (*n* = 2), Tfh (*n* = 2), central memory T cells (T_{CM}) (*n* = 2), effector memory T cells (T_{EM}) (*n* = 2), cord blood versus PB (*n* = 1), resting Tregs (*n* = 1), activated Tregs (*n* = 1), resting memory cells (*n* = 1), and a population enriched in Th17 (*n* = 1).

Th1 cells currently most frequently associated with superior antitumor immune responses. In BC, the majority of previous investigations focusing on CD4+ T cells have examined the suppressive activities of Tregs in dampening immune functions (24).

This study was undertaken to characterize the CD4+ T cell subpopulations infiltrating human breast tumors in a direct ex vivo analysis of fresh tumor tissue without enzymatic digestion or short-term in vitro expansion. We profiled gene expression in purified CD4+ T cells from the primary tumors (referred to herein as TIL), axillary LN, and peripheral blood (PB) to produce global images of these cells in their native state. An important finding from our work is that extensively infiltrated tumors are less immunosuppressive and have a higher frequency of organized LN-like structures associated with detectable CXCL13-producing CD4+ follicular helper T (Tfh) cells. Tertiary lymphoid structures (TLS) have been previously identified in lung and colorectal cancers, and their presence has been linked with positive patient prognosis (25–27). In this study we show that Tfh cells are an important constituent of TLS in breast tumors. Animal models have demonstrated that Tfh cells in LNs are highly activated and participate in various steps leading to germinal center (GC) development and differentiation of memory B and antibody-secreting plasma cells (28). The data presented here suggest that CXCL13-producing Tfh TIL may play an important role in immune cell recruitment to the tumor microenvironment and influence TLS formation, thereby helping to create a haven in the tumor mass in which effective and durable antitumor immune responses can be generated.

Results

The immune infiltrate in BC. Freshly resected invasive breast tumor tissue from systemically untreated patients (a graphical overview for navigating the experimental data is provided in Supplemental Table 1A; supplemental material available online with this article; doi:10.1172/JCI67428DS1; clinicopathological characteristics for the patient discovery set [*n* = 10] in Supplemental Table 1B and patient confirmation set [*n* = 60] in Supplemental Table 1C) was rapidly mechanically dissociated into a single cell homogenate using the GentleMACS system for immediate ex vivo analysis following CD4+ T cell isolation. The distribution of infiltrating CD45+ cells (Supplemental Figure 1) included a majority of T cells (±75%; range = 60%–90%) together with <20% B cells, <10% monocytes, <5% NK cells, or NKT cells, similar to a recently published study (29). Among the CD3+ T cells, the CD4+ subset was consistently the principal component (Figure 1A; mean = 53% in 35 tumors), outnumbering CD8+ T cells and present both at a higher frequency and ratio than in ipsilateral nonadjacent normal breast tissue (mean = 38% in 31 samples).

Features of the CD4+ T cell infiltrate. Global gene expression profiles of the TIL were compared with CD4+ T cells from patient's axillary LN and PB (P-PB) and PB from healthy donors (D-PB) (Supplemental Table 1B). Bootstrap analysis revealed stable groupings by tissue type, with patient and donor blood segregating together (Figure 1B). This observation could be partially due to differences in the ratio of naive (CD45RA+) to memory (CD45RO+) CD4+ T cells, with generally about 50% CD45RO+ in PB, >50% in LN, and >95% in TIL (expression of the 58 Th surface markers investigated was also examined on naive and memory donor CD3+CD4+ T cells as a control; Supplemental Figure 2). The gene expression profiles were analyzed in a variety of comparisons, including TIL compared with LN or P-PB, P-PB compared with D-PB, and ER+ compared with ER– tumors (Supplemental Table 2). The extent of the CD4+ T cell infiltrate (IHC; Supplemental Table 1B) revealed that 2 ER+ and 2 ER– tumors were extensively infiltrated while 3 ER+ and 3 ER– tumors were minimally infiltrated, with these groups also compared. Our analyses initially (a) concluded that the CD4+ T cell profiles were remarkably similar between P-PB and D-PB (Supplemental Table 2E), with the autologous cells constituting a good internal control; (b) found surprisingly few gene changes between ER+ and ER– tumors (Supplemental Table 2F); and (c) detected important differences in immune response genes between extensively and minimally infiltrated tumors (Supplemental Table 2G), which will be detailed throughout this article (extensively infiltrated is defined as overall >5% intratumoral and >10% stromal lymphocytes in multiple sections of the resected invasive tumor; criteria detailed in Supplemental Table 1C).

Molecular images of the CD4+ Th subsets present in the TIL were produced by comparing our patient data with public Th gene expression data sets (refs. 30–32; reanalyzed applying our small group criteria [ref. 33] which are detailed in the Supplemental Methods). Our innovative use of these public data sets allowed us to detect the presence of each CD4+ T cell subpopulation in the TIL and extend the individual Th subset profiles beyond conventional markers with relative specificity. A direct comparison of patient CD4+ T cell data with the public Th gene lists produced distinct gene sets (Figure 1, C–H; Figure 2, A–C; and Supplemental Table 3) showing that (a) D-PB and P-PB are relatively similar across all Th subsets, with a slight increase in effector memory cell markers in P-PB; (b) LN profiles are transitional between P-PB and TIL, with upregulation of the Tfh genes *CD200*, *CXCL13*, and *ICOS* and the Th1 genes *CD38* (34), *CXCL9*, *IFNG*, and *IL2*, which are notably among the limited number of gene alterations detected (Figure 3); (c) the TIL profile is enriched in all major Th subpopulations (Th1, Th2, Tfh, Treg, and Th17); (d) the TIL are activated CD25+ cells; and (e) the TIL have a memory phenotype closer to that of effector than that of central memory cells. Expression levels of conventional Th markers (Supplemental Table 3K) reiterated that all Th subpopulations were

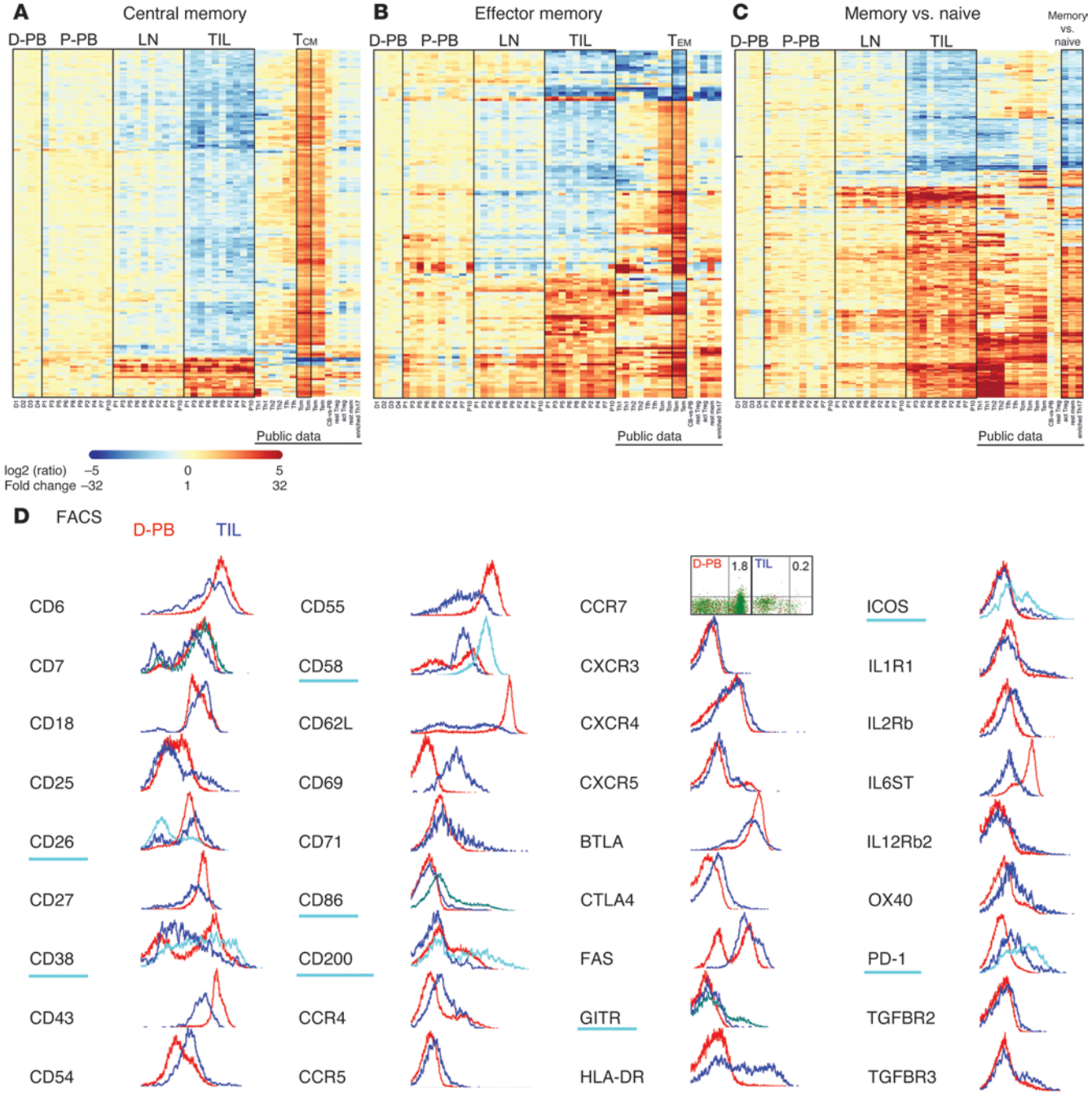

Figure 2

Characteristics of CD4+ T cells infiltrating breast tumors. Purified CD4+ T cells were from fresh tumor homogenates, LNs, P-PB, or D-PB (patient discovery set; Supplemental Table 1B). (**A**–**C**) Statistically significant gene changes established for the comparison of TIL versus P-PB (Supplemental Table 2B) were compared with public microarray data sets of human Th subpopulations that we reanalyzed (Supplemental Methods) as in Figure 1, C–H. (**D**) Histogram or dot plot thumbnails for 36 Th surface markers (genes in **A**–**C** and Figure 1, C–H; complete profiles plus 24 additional markers in Supplemental Figure 2) expressed on CD4+ TIL (variation is indicated by shades of blue) and D-PB (red). The genes underlined in aqua were also analyzed by qRT-PCR on a larger patient group (Figure 8).

present in the TIL but did not provide definite information on their relative distribution. Alternatively, the comparison of TIL from extensively versus minimally infiltrated tumors revealed a distinct skew to Tfh (*CD200*, *CXCL13*, *ICOS*, and *PDCD1* [known as *PD-1*]) and Th1 (*CD38*, *CXCL9*, *CXCL10*, *CXCL11*, *IFNG*, and *TBX21* [also known as *T-bet*]) gene expression in the extensively infiltrated tumors (Figure 3). The Treg marker *FOXP3* was also increased in extensively versus minimally infiltrated tumors (Figure 3), but the Treg produced ligand *TGFB2* was decreased in this comparison (both were significantly increased in TIL com-

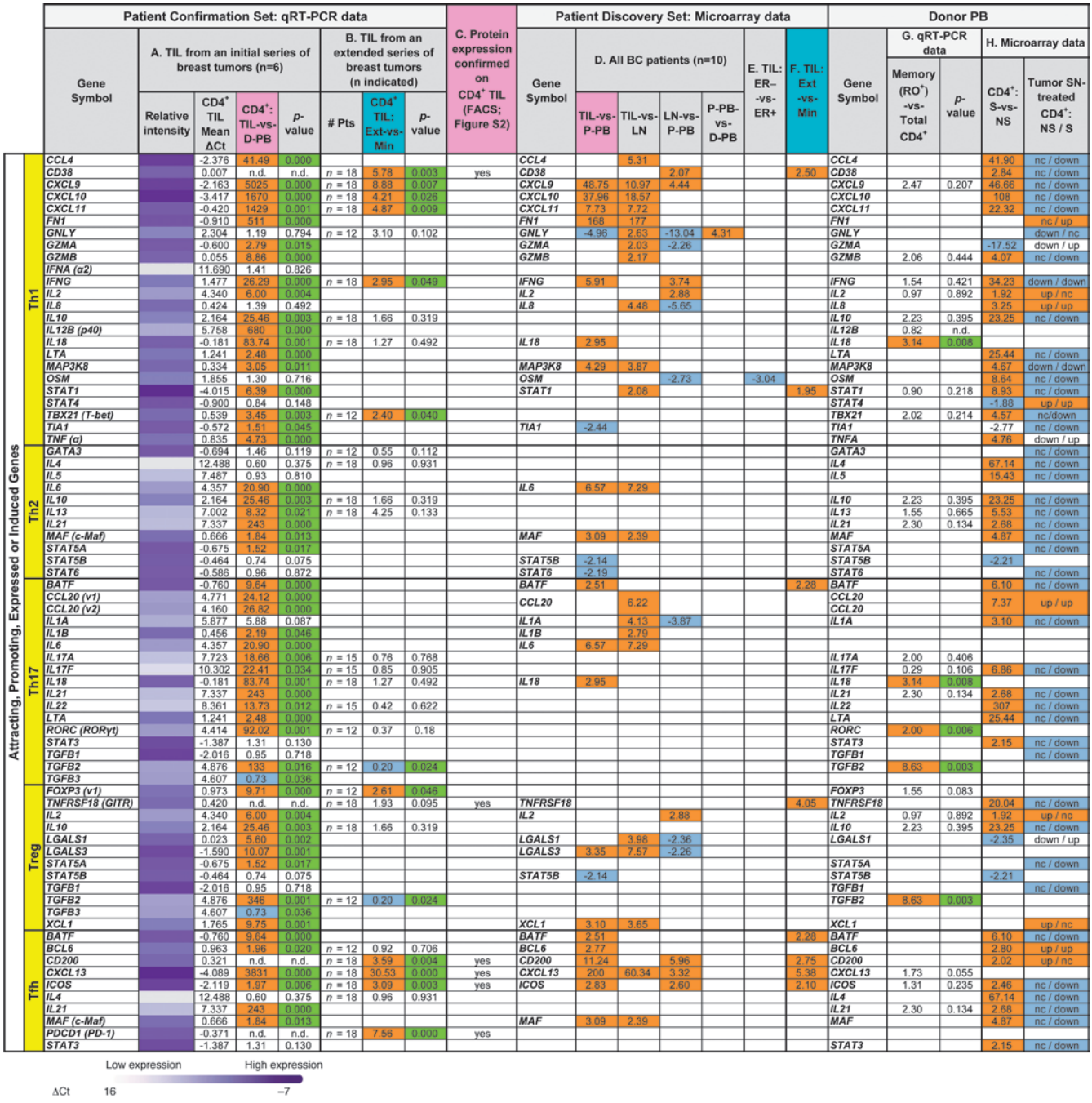

		Gene Symbol	A. TIL from an initial series of breast tumors (n=6) Relative intensity	CD4+ TIL Mean ΔCt	CD4+: TIL-vs-D-PB	p-value	B. TIL from an extended series of breast tumors (n indicated) # Pts	CD4+ TIL: Ext-vs-Min	p-value	C. Protein expression confirmed on CD4+ TIL (FACS; Figure S2)	Gene Symbol	D. All BC patients (n=10) TIL-vs-P-PB	TIL-vs-LN	LN-vs-P-PB	P-PB-vs-D-PB	E. TIL: ER–-vs-ER+	F. TIL: Ext-vs-Min	Gene Symbol	G. qRT-PCR data Memory (RO+)-vs-Total CD4+	p-value	H. Microarray data CD4+: S-vs-NS	Tumor SN-treated CD4+: NS / S
Attracting, Promoting, Expressed or Induced Genes	Th1	CCL4		-2.376	41.49	0.000					CCL4		5.31					CCL4			41.90	nc / down
		CD38		0.007	n.d.	n.d.	n = 18	5.78	0.003	yes	CD38			2.07			2.50	CD38			2.84	nc / down
		CXCL9		-2.163	5025	0.000	n = 18	8.88	0.007		CXCL9	48.75	10.97	4.44				CXCL9	2.47	0.207	46.66	nc / down
		CXCL10		-3.417	1670	0.000	n = 18	4.21	0.026		CXCL10	37.96	18.57					CXCL10			108	nc / down
		CXCL11		-0.420	1429	0.001	n = 18	4.87	0.009		CXCL11	7.73	7.72					CXCL11			22.32	nc / down
		FN1		-0.910	511	0.000					FN1	168	177					FN1				nc / up
		GNLY		2.304	1.19	0.794	n = 12	3.10	0.102		GNLY	-4.96	2.63	-13.04	4.31			GNLY				down / nc
		GZMA		-0.600	2.79	0.015					GZMA		2.03	-2.26				GZMA			-17.52	down / up
		GZMB		0.055	8.86	0.000					GZMB		2.17					GZMB	2.06	0.444	4.07	nc / down
		IFNA (α2)		11.690	1.41	0.826																
		IFNG		1.477	26.29	0.000	n = 18	2.95	0.049		IFNG	5.91		3.74				IFNG	1.54	0.421	34.23	down / down
		IL2		4.340	6.00	0.004					IL2			2.88				IL2	0.97	0.892	1.92	up / nc
		IL8		0.424	1.39	0.492					IL8		4.48	-5.65				IL8			3.25	up / up
		IL10		2.164	25.46	0.003	n = 18	1.66	0.319									IL10	2.23	0.395	23.25	nc / down
		IL12B (p40)		5.758	680	0.000												IL12B	0.82	n.d.		
		IL18		-0.181	83.74	0.001	n = 18	1.27	0.492		IL18	2.95						IL18	3.14	0.008		
		LTA		1.241	2.48	0.000												LTA			25.44	nc / down
		MAP3K8		0.334	3.05	0.011					MAP3K8	4.29	3.87					MAP3K8			4.67	down / down
		OSM		1.855	1.30	0.716					OSM			-2.73		-3.04		OSM			8.64	nc / down
		STAT1		-4.015	6.39	0.000					STAT1		2.08				1.95	STAT1	0.90	0.218	8.93	nc / down
		STAT4		-0.900	0.84	0.148												STAT4			-1.88	up / up
		TBX21 (T-bet)		0.539	3.45	0.003	n = 12	2.40	0.040									TBX21	2.02	0.214	4.57	nc/down
		TIA1		-0.572	1.51	0.045					TIA1	-2.44						TIA1			-2.77	nc / down
		TNF (α)		0.835	4.73	0.000												TNFA			4.76	down / up
	Th2	GATA3		-0.694	1.46	0.119	n = 12	0.55	0.112									GATA3				nc / down
		IL4		12.488	0.60	0.375	n = 18	0.96	0.931									IL4			67.14	nc / down
		IL5		7.487	0.93	0.810												IL5			15.43	nc / down
		IL6		4.357	20.90	0.000					IL6	6.57	7.29									
		IL10		2.164	25.46	0.003	n = 18	1.66	0.319									IL10	2.23	0.395	23.25	nc / down
		IL13		7.002	8.32	0.021	n = 18	4.25	0.133									IL13	1.55	0.665	5.53	nc / down
		IL21		7.337	243	0.000												IL21	2.30	0.134	2.68	nc / down
		MAF (c-Maf)		0.666	1.84	0.013					MAF	3.09	2.39					MAF			4.87	nc / down
		STAT5A		-0.675	1.52	0.017												STAT5A				nc / down
		STAT5B		-0.464	0.74	0.075					STAT5B	-2.14						STAT5B			-2.21	
		STAT6		-0.586	0.96	0.872					STAT6	-2.19						STAT6				nc / down
	Th17	BATF		-0.760	9.64	0.000					BATF	2.51					2.28	BATF			6.10	nc / down
		CCL20 (v1)		4.771	24.12	0.000					CCL20		6.22					CCL20			7.37	up / up
		CCL20 (v2)		4.160	26.82	0.000												CCL20				
		IL1A		5.877	5.88	0.087					IL1A		4.13	-3.87				IL1A			3.10	nc / down
		IL1B		0.456	2.19	0.046					IL1B		2.79									
		IL6		4.357	20.90	0.000					IL6	6.57	7.29									
		IL17A		7.723	18.66	0.006	n = 15	0.76	0.768									IL17A	2.00	0.406		
		IL17F		10.302	22.41	0.034	n = 15	0.85	0.905									IL17F	0.29	0.106	6.86	nc / down
		IL18		-0.181	83.74	0.001	n = 18	1.27	0.492		IL18	2.95						IL18	3.14	0.008		
		IL21		7.337	243	0.000												IL21	2.30	0.134	2.68	nc / down
		IL22		8.361	13.73	0.012	n = 15	0.42	0.622									IL22			307	nc / down
		LTA		1.241	2.48	0.000												LTA			25.44	nc / down
		RORC (RORγt)		4.414	92.02	0.001	n = 12	0.37	0.18									RORC	2.00	0.006		
		STAT3		-1.387	1.31	0.130												STAT3			2.15	nc / down
		TGFB1		-2.016	0.95	0.718												TGFB1				nc / down
		TGFB2		4.876	133	0.016	n = 12	0.20	0.024									TGFB2	8.63	0.003		
		TGFB3		4.607	0.73	0.036																
	Treg	FOXP3 (v1)		0.973	9.71	0.000	n = 12	2.61	0.046									FOXP3	1.55	0.083		
		TNFRSF18 (GITR)		0.420	n.d.	n.d.	n = 18	1.93	0.095	yes	TNFRSF18						4.05	TNFRSF18			20.04	nc / down
		IL2		4.340	6.00	0.004					IL2			2.88				IL2	0.97	0.892	1.92	up / nc
		IL10		2.164	25.46	0.003	n = 18	1.66	0.319									IL10	2.23	0.395	23.25	nc / down
		LGALS1		0.023	5.60	0.002					LGALS1		3.98	-2.36				LGALS1			-2.35	down / up
		LGALS3		-1.590	10.07	0.001					LGALS3	3.35	7.57	-2.26								
		STAT5A		-0.675	1.52	0.017												STAT5A				nc / down
		STAT5B		-0.464	0.74	0.075					STAT5B	-2.14						STAT5B			-2.21	
		TGFB1		-2.016	0.95	0.718												TGFB1				nc / down
		TGFB2		4.876	346	0.001	n = 12	0.20	0.024									TGFB2	8.63	0.003		
		TGFB3		4.607	0.73	0.036																
		XCL1		1.765	9.75	0.001					XCL1	3.10	3.65					XCL1				up / nc
	Tfh	BATF		-0.760	9.64	0.000					BATF	2.51					2.28	BATF			6.10	nc / down
		BCL6		0.963	1.96	0.020	n = 12	0.92	0.706		BCL6	2.77						BCL6			2.80	up / up
		CD200		0.321	n.d.	n.d.	n = 18	3.59	0.004	yes	CD200	11.24		5.96			2.75	CD200			2.02	up / nc
		CXCL13		-4.089	3831	0.000	n = 18	30.53	0.000	yes	CXCL13	200	60.34	3.32			5.38	CXCL13	1.73	0.055		
		ICOS		-2.119	1.97	0.006	n = 18	3.09	0.003	yes	ICOS	2.83		2.60			2.10	ICOS	1.31	0.235	2.46	nc / down
		IL4		12.488	0.60	0.375	n = 18	0.96	0.931									IL4			67.14	nc / down
		IL21		7.337	243	0.000												IL21	2.30	0.134	2.68	nc / down
		MAF (c-Maf)		0.666	1.84	0.013					MAF	3.09	2.39					MAF			4.87	nc / down
		PDCD1 (PD-1)		-0.371	n.d.	n.d.	n = 18	7.56	0.000	yes												
		STAT3		-1.387	1.31	0.130												STAT3			2.15	nc / down

Low expression — High expression

ΔCt 16 –7

Figure 3

Conventional Th subset marker expression in TIL. (**A**–**C**) Th subset marker genes were quantified in the patient confirmation set by (**A** and **B**) qRT-PCR and (**C**) flow cytometry. (**A**) Mean ΔCt values (relative to the Th-specific endogen CASC3) are inversely proportional to the relative intensity of gene expression; CD4+ TIL (n = 6) are compared with D-PB (n = 6). (**B**) CD4+ TIL from extensively infiltrated tumors (n = 6) are compared with minimally infiltrated tumors (n = 12). "n = <18" indicates that the number of minimally infiltrated tumors assessed was as noted. (**C**) Protein expression was assessed by flow cytometry (Supplemental Figure 2). (**D**–**F**) Microarray data from the patient discovery set and (**G**) qRT-pCR data of memory versus total CD4+ T cells from healthy donor cells are shown for comparison with (**D**) CD4+ T cells isolated from the first tissue (i.e., TIL) relative to the second tissue (i.e., P-PB), (**E**) CD4+ T cells isolated from ER– relative to ER+ tumors, (**F**) CD4+ T cells isolated from extensively infiltrated tumors relative to minimally infiltrated tumors, and (**G**) D-PB CD4+CD45RO+ memory T cells (n = 3) compared with total CD4+ T cells (n = 3). (**H**) Microarray data of D-PB memory CD4+ T cells after S or tumor SN treatment (Figure 6 and Supplemental Table 6). Fold change or ratio values are shown as blue (downregulated) and orange (upregulated); P values (2-tailed Student's t test with unequal variance) in green are significant (P < 0.05); n.d., not determined (for qRT-PCR data no data = n.d.); nc, no change (for microarray data empty cells = nc). For gene symbols, "v" indicates transcript variant.

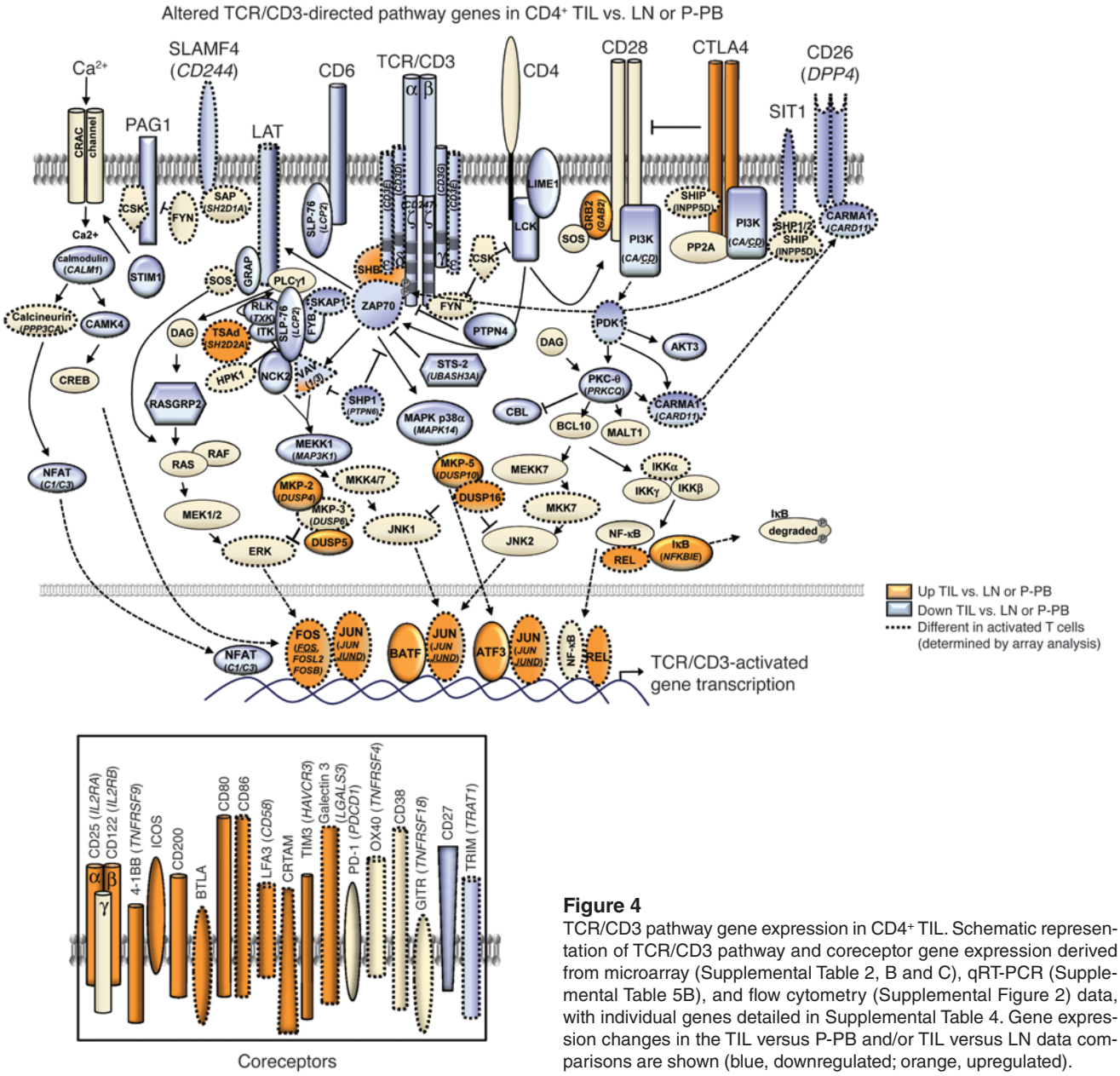

Figure 4
TCR/CD3 pathway gene expression in CD4+ TIL. Schematic representation of TCR/CD3 pathway and coreceptor gene expression derived from microarray (Supplemental Table 2, B and C), qRT-PCR (Supplemental Table 5B), and flow cytometry (Supplemental Figure 2) data, with individual genes detailed in Supplemental Table 4. Gene expression changes in the TIL versus P-PB and/or TIL versus LN data comparisons are shown (blue, downregulated; orange, upregulated).

pared with D-PB). This suggests that the observed increase in *FOXP3* expression may be related to its transient expression by activated Th cells rather than a greater presence of Tregs in the extensively infiltrated tumors.

Flow cytometric analysis of $CD4^+$ TIL from additional patients with BC compared with $CD4^+$ T cells from healthy donor blood (Supplemental Table 1C) largely validated these data and provided more quantitative information, demonstrating that the $CD4^+$ TIL are antigen-experienced effector memory cells ($CD45RO^+$), characterized either wholly or in a subpopulation of cells as $TCR/CD3^{lo}$ $CD6^{lo}$ $CD7^{lo}$ $CD11b^+$ $CD18^+$ $CD24^+$ $CD25^+$ $CD26^+$ $CD27^{lo}$ $CD28^{lo}$ $CD35^-$ $CD38^+$ $CD43^{lo}$ $CD44^+$ $CD49D^+$ $CD54^{hi}$ $CD55^{lo}$ $CD57^{lo}$ $CD58^{hi}$ $CD59^+$ $CD62L^{lo}$ $CD69^+$ $CD71^+$ $CD73^+$ $CD80^+$ $CD86^+$ $CD109^+$ $CD146^+$ $CD166^+$ $CD200^+$ $CCR4^+$ $CCR5^+$ $CCR6^{lo}$ $CCR7^{lo}$ $CX3CR1^{lo}$ $CXCR3^+$ $CXCR4^+$ $CXCR5^+$ 4-1BB$^+$ BTLA$^+$ CRTH2$^+$ CTLA4$^+$ FAS^{hi} GITR$^+$ HLA-DR$^+$ $ICOS^+$ IL1R1$^+$ IL2RB$^+$ $IL6ST^{lo}$ IL7R$^+$ IL12RB2$^+$ IL17RB$^+$ IL17RD$^+$ OX40$^+$ OX40L$^+$ PD-1$^+$ TGFBR2$^+$ TGFBR3$^+$ (Supplemental Figure 2). The heterogeneity observed in some activation-induced markers (e.g., CD25, CD71, HLA-DR) suggests that not all of the cells are activated. Upregulation of conventional Th surface markers on $CD4^+$ TIL subpopulations was detected (Supplemental Figure 2) and included (a) the Tfh-associated BTLA, $CD200^{hi}$, ICOS, and $PD\text{-}1^{hi}$; (b) the Th1-associated $CD38^{hi}$, CCR5, CD54, and IL12RB2; (c) the Th2-associated CCR4; (d) the Th17-associated IL1R1; and (e) the Treg-associated $CD25^{hi}$ and GITR. Histogram or dot plot thumbnails are shown for Th surface marker genes present in the Figure 1, C–H, and Figure 2, A–C, heat maps (Figure 2D; full histograms or dot plots in Supplemental Figure 2). Interestingly, among differentially expressed surface markers

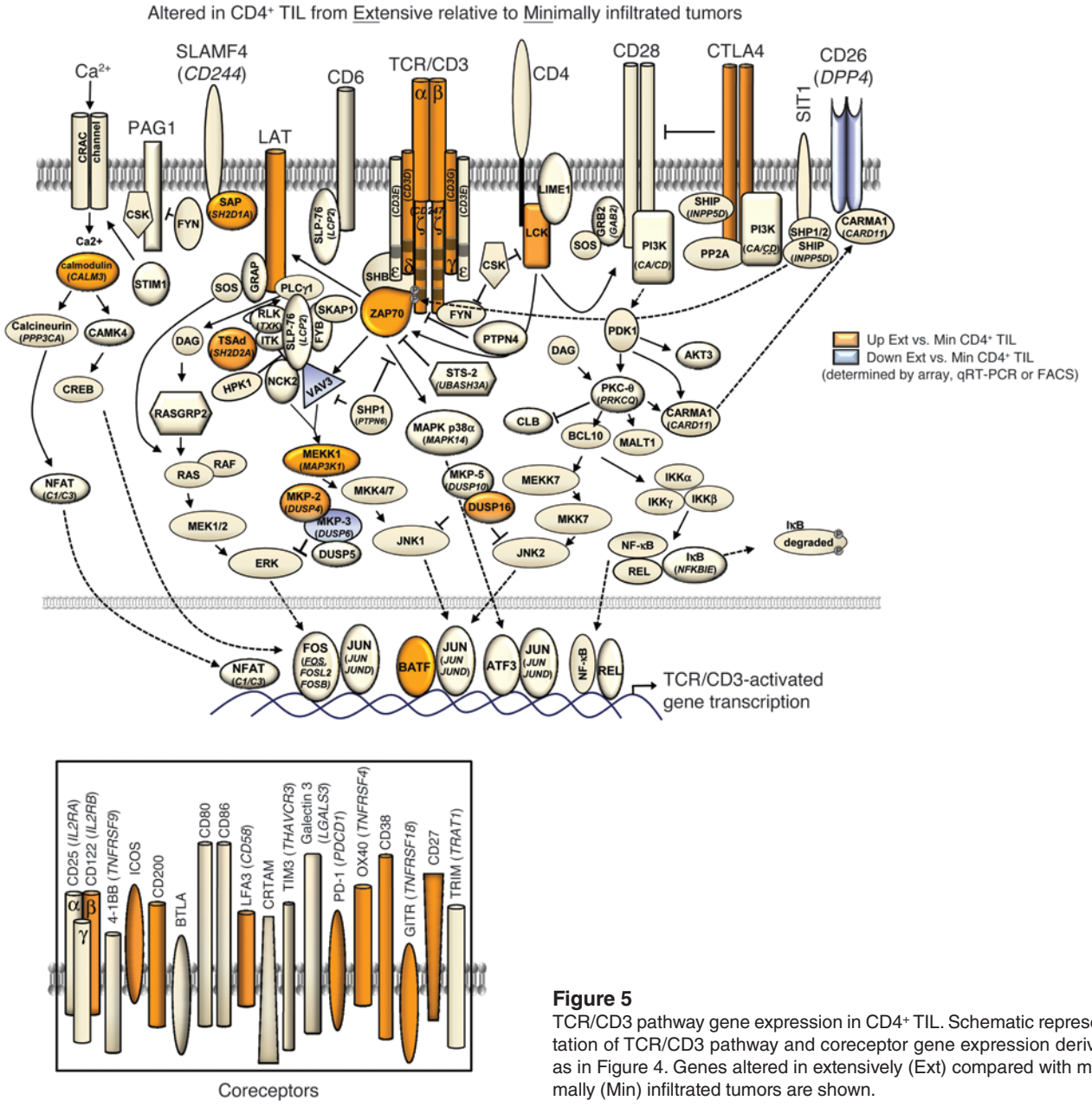

Figure 5
TCR/CD3 pathway gene expression in CD4+ TIL. Schematic representation of TCR/CD3 pathway and coreceptor gene expression derived as in Figure 4. Genes altered in extensively (Ext) compared with minimally (Min) infiltrated tumors are shown.

(Figure 2D, underlined in blue), CD38, CD200, ICOS, and PD-1 expression was higher on CD4+ TIL from extensively infiltrated tumors, which was confirmed at the mRNA level (Figure 3).

Many of the gene and surface markers expressed on some or all of the TIL reflect an activated state; however, only low levels of Th-derived cytokines/chemokines had statistically significant increases in the TIL versus P-PB comparison (Figure 3). Analyses using more sensitive quantitative PCR with reverse transcription (qRT-PCR) confirmed these gene expression increases and expanded the set of expressed Th-derived factors (Tfh [*CXCL13* and *IL21*], Th1 [*CXCL9*, *CXCL10*, *CXCL11*, *GZMA*, *GZMB*, *IFNG*, and *IL2*], Th2 [*IL13*], Th17 [*CCL20*, *IL17A*, *IL17F*, *IL21*, and *IL22*], and Tregs [*IL10*, *TGFB*, and *XCL1*]), although many were not at stimulation-induced (S-induced) levels (microarray data), with reduced expression more pronounced in minimal relative to extensively infiltrated tumors. These data indicate that while all Th subsets are infiltrating BC, the full complement of Th cytokines/chemokines is not produced.

Concurrent activation and suppression. The lack of robust or comprehensive cytokine/chemokine expression by the CD4+ TIL led us to investigate the nature of their activation state. Evaluation of prototypic TCR/CD3 pathway genes identified a substantial number that were downregulated in the TIL compared with their counterparts from LN or P-PB (Figure 4). This suppression includes components of the TCR/CD3 complex, molecules involved in signal transduction, costimulatory receptors, transcription factors, and negative regulatory molecules (genes detailed in Supplemental Table 4). Some of these gene changes were confirmed at the mRNA (Supplemental Table 5B) or protein levels (Supplemental Figure 2). TCR/CD3 downregulation

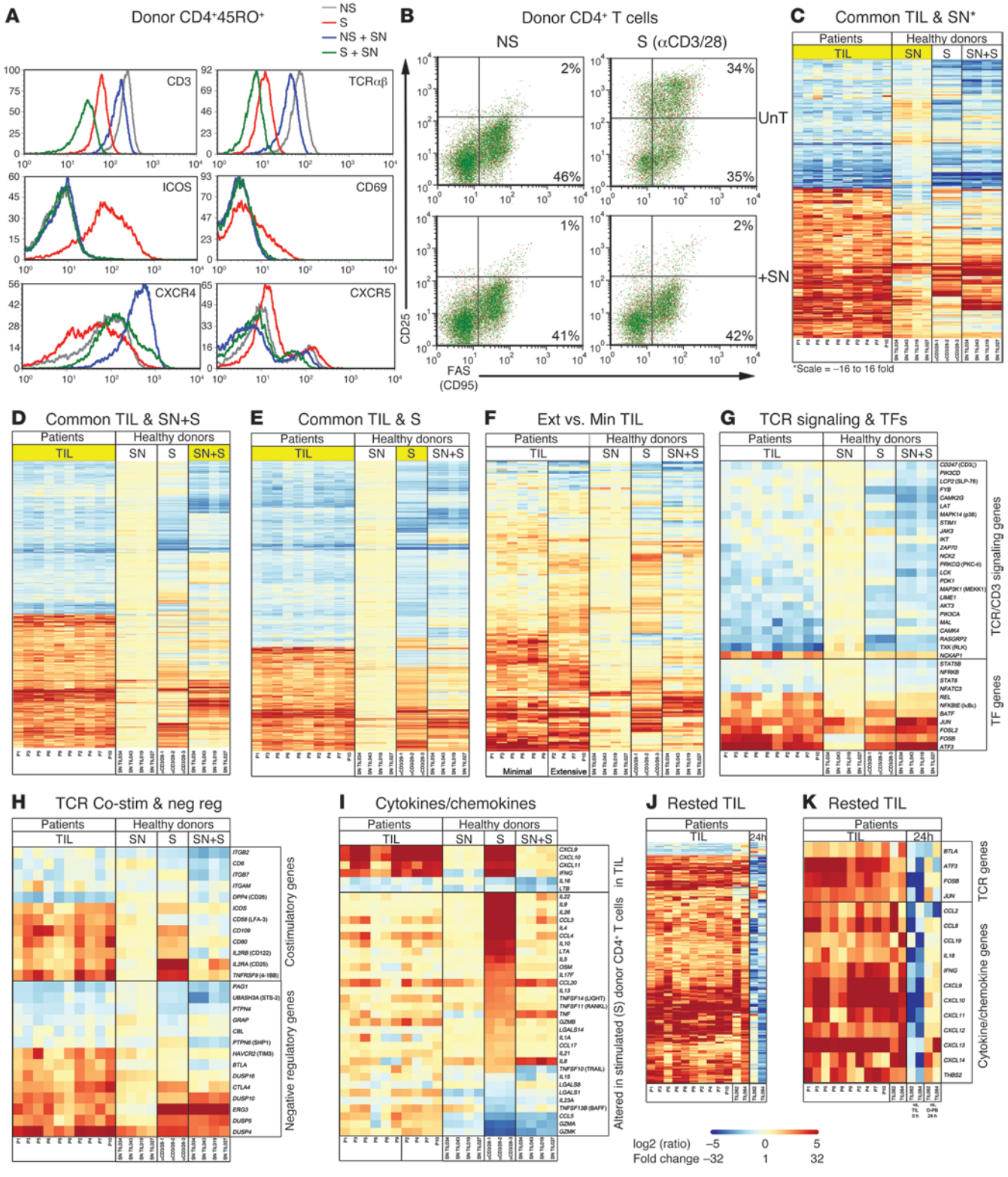
A
Donor CD4+45RO+
NS
S
NS + SN
S + SN
CD3
TCRαβ
ICOS
CD69
CXCR4
CXCR5
B
Donor CD4+ T cells
NS
S (αCD3/28)
2%
34%
46%
35%
1%
2%
41%
42%
UnT
+SN
CD25
FAS (CD95)
C
Common TIL & SN*
Patients
Healthy donors
TIL
SN
S
SN+S
*Scale = −16 to 16 fold
D
Common TIL & SN+S
E
Common TIL & S
F
Ext vs. Min TIL
Minimal
Extensive
G
TCR signaling & TFs
TCR/CD3 signaling genes
TF genes
H
TCR Co-stim & neg reg
Costimulatory genes
Negative regulatory genes
I
Cytokines/chemokines
Altered in stimulated (S) donor CD4+ T cells in TIL
J
Rested TIL
24h
K
Rested TIL
TCR genes
Cytokine/chemokine genes
log2 (ratio) −5 0 5
Fold change −32 1 32

Figure 6
Tumor SN suppresses activation of donor CD4+ T cells. D-PB CD4+ T cells (unstimulated or S) were treated for 24 hours with primary tumor SN. Expression of activation markers on (**A**) CD4+CD45RO+ T cells or (**B**) total CD4+ T cells. (**C**–**I**) TIL gene expression data (P1–P10) was compared with donor CD4+CD45RO+ T cells treated with SN with or without S (SN = 2 minimal [TIL034 and TIL043] and 2 extensive [TIL019 and TIL027; the latter is borderline extensive, Supplemental Table 1C] tumors; Supplemental Table 1C). Heat maps show genes commonly altered in TIL and donor cells treated with SN with or without S for the designated comparison (red, upregulated; blue, downregulated). Samples include TIL from minimally (P1, P3, P5, P6, P8, P9) and extensively (P2, P4, P7, P10) infiltrated tumors; SN-treated (n = 4), S-treated (n = 3), and SN+S-treated (n = 4) D-PB. Genes commonly altered in P1–P10 TIL versus their P-PB and (**C**) SN-treated, (**D**) SN+S-treated, or (**E**) S-treated donor cells are highlighted. (**F**) Genes differentially expressed in TIL from extensively versus minimally infiltrated tumors and altered by SN or S+SN treatment are highlighted. Select TCR/CD3 pathway genes include (**G**) signaling molecules and targeted transcription factors; (**H**) costimulatory receptors and negative regulatory genes; and (**I**) cytokine/chemokine genes. (**J** and **K**) Freshly isolated CD4+ TIL from patients (TIL062 and TIL064; Supplemental Table 1C) and CD4+ memory T cells from D-PB were immediately extracted or rested for 24 hours. Specific gene changes in the two rested TIL were compared with P1–P10 TIL. Expression levels for the commonly altered genes are shown in **J**, with specific TCR/CD3 pathway and cytokine/chemokine genes highlighted in **K**.

on TIL has been described for a wide variety of solid tumors (35), but the depth of this suppression, extending through the signaling pathway and divergent from activation-induced modifications, has not been previously reported. A comparison with gene expression profiles of stimulated donor CD4+CD45RO+ T cells revealed that only approximately 50% were similarly induced or repressed by TCR/CD3 activation (Figure 4 and Supplemental Table 4). The disparity with T cell activation is highlighted by the number of aberrantly expressed coreceptors, which are involved in regulating the TCR/CD3 signal. Interestingly, the NF-κB transcription factor *REL* and members of the AP-1 family (*ATF3*, *BATF*, *FOSB*/*FOSL2*, and *JUN*/*JUND* were specifically upregulated despite reduced upstream MAPK signaling. *REL* and some AP-1 transcription factor genes were increased in the LN profiles but to a lesser degree (Supplemental Table 2D). An indication that this overall pattern of TCR/CD3 signaling gene expression may be significant is highlighted by the differences observed in extensively versus minimally infiltrated tumors (Figure 5). Extensively infiltrated tumors are characterized by higher expression of the TCR/CD3 subunits and numerous coreceptor genes (including *CD38*, *CD200*, *ICOS*, and *PDCD1*) as well as many signaling genes (including *ZAP70*) (Figure 3, Supplemental Figure 2, Supplemental Table 4, and Supplemental Table 5B). These data suggest that extensively infiltrated tumors are characterized by lower levels of TCR/CD3 suppression and/or higher levels of T cell activation.

We next performed a series of in vitro experiments to explore this combination of activation and suppression. CD4+ CD45RO+ (or total CD4+) T cells from D-PB were treated with supernatant (SN) retained from fresh primary tumor homogenates, alone or in conjunction with S. SN downregulated TCR/CD3 expression and inhibited activation-induced surface receptor expression, characterized by CD69, ICOS, CD25, and FAS (Figure 6, A and B). SN also reduced expression of CXCR5, the receptor for CXCL13, a chemokine that plays an important role in homing to B cell follicles (36). Alternatively, SN and to a lesser degree SN plus S (SN+S), induced expression of CXCR4, the receptor for CXCL12 whose protumor activities are well documented (37). Gene expression arrays revealed that approximately 75% of the genes commonly altered in the TIL and their SN-treated donor PB counterparts were either similarly upregulated or downregulated (Figure 6C and Supplemental Table 6B). Expression profiles of the donor SN-treated cells (versus untreated cells) were compared with the TIL versus P-PB data, clearly demonstrating that the SN effect is appreciably amplified by S, with the SN+S cells (Figure 6D and Supplemental Table 6C) more closely resembling the TIL than SN alone (Figure 6, C–E). The SN+S gene profiles are also distinct from those of S alone (Figure 6E and Supplemental Table 6D) and largely reiterate a mixed pattern of activation and suppression.

Closer examination of the SN+S effect on TCR/CD3 pathway genes (Figure 6, G and H, and Supplemental Table 4) detected (a) significant suppression of various signaling genes that was more pronounced than that in the S donor cells; (b) specific upregulation of *REL* and AP-1/ATF family transcription factors similar to that in the TIL; (c) more potent suppression of a subset of costimulatory receptor genes compared with that in the TIL or S donor cells; and (d) a pattern of negative regulatory gene expression that was similar between the SN+S and S donor cells. Additionally, the SN+S treatment suppressed most of the S-induced changes detected in S counterparts, including expression of the majority of detected cytokines/chemokines (Figure 6I and Supplemental Table 6E). Among the Th cytokines/chemokines produced in the S donor cells, only the proinflammatory, tumor-promoting factors *CCL20*, *IL8*, and *TNF* were further upregulated by SN+S treatment. *IFNG* and the IFN-γ–induced chemokines *CXCL9*, *CXCL10*, and *CXCL11* were the only S-induced factors also expressed in the TIL, with their overt suppression by SN+S potentially reflecting a stronger effect from higher local concentrations in vitro. This interpretation is reinforced by the observed SN-mediated suppression of *CXCR3* (the receptor for CXCL9, CXCL10, and CXCL11; ref. 37 and Supplemental Table 6H) in parallel with *CXCR4* upregulation in unstimulated or S donor cells (Figure 6A). Overall, these data support the view that the simultaneously activated/suppressed TIL profile is broadly reproduced by SN+S treatment of donor CD4+ T cells, where the suppressive SN effect is amplified by S.

To determine whether these tumor-mediated effects on CD4+ T cells were transient, freshly isolated TIL were split and either extracted immediately or "rested" ex vivo overnight without S. Gene expression profiling shows the rested TIL reverse expression in a sizable number of genes expressed in their freshly isolated counterparts (Figure 6, J and K, and Supplemental Table 6F). Notably, the cytokine/chemokine genes, including *IFNG* and IFN-γ–induced genes, were upregulated in the TIL and returned to baseline 24 hours after removal from the tumor microenvironment. An exception was the B cell chemoattractant *CXCL13*, for which the high TIL expression levels decreased only by 50% at 24 hours, with the rested TIL from an extensively infiltrated tumor (TIL064) still expressing CXCL13 at substantially higher levels (159-fold increase) compared with memory D-PB control. Reversal of altered TCR/CD3 pathway gene expression in the rested TIL was limited to *BTLA* and the AP-1 factors *ATF3*, *FOSB*, and *JUN*, suggesting that suppression of TCR/CD3 signaling is not fully relieved at 24 hours. Additionally, these in vitro experiments show that the

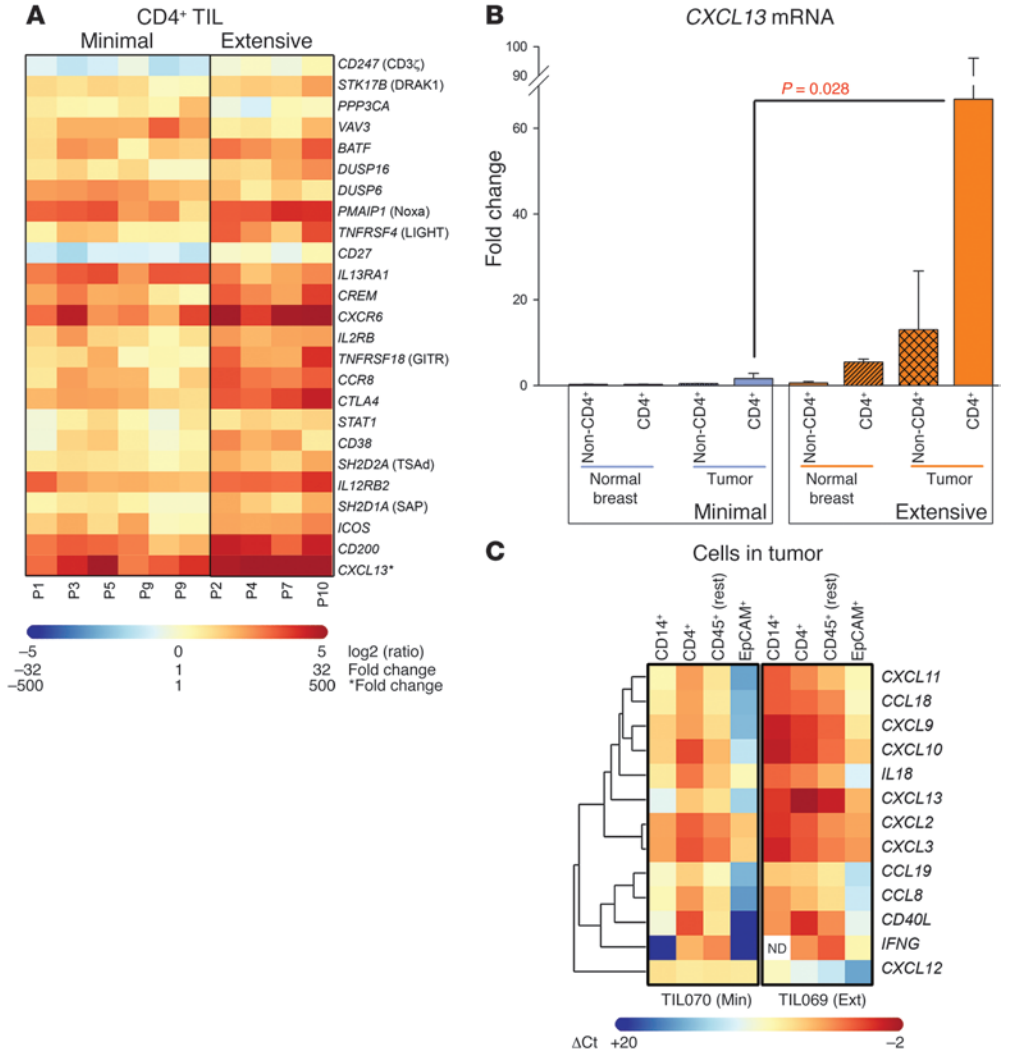

Figure 7

Genes predominately expressed in CD4+ TIL from extensively and minimally infiltrated tumors. (**A**) Heat map (red, upregulated; blue, downregulated) for a select group of differentially expressed genes in extensively compared with minimally infiltrated tumors (P1–P10 TIL; Supplemental Table 2G), including TCR/CD3 pathway, activation-induced, and conventional Th subset marker genes. Due to its high expression levels, the scale for CXCL13 is different. (**B**) *CXCL13* transcript levels determined by qRT-PCR (normalized to *TMBIM4* [endogen]) in either CD4+ or non-CD4 cells (remaining cells in CD4-depleted homogenates) from tumors and normal breast tissue ($n = 6$; 3 extensive [orange], 3 minimal [blue]; fold changes were normalized to the 3 minimal CD4+ cells). *P* values were calculated for several comparisons (Supplemental Table 5E), with the *P* value for CD4+ TIL (Ext vs. Min) shown (mean ± SEM). (**C**) CD14+ (monocyte), CD4+, remaining CD45+ (other leukocytes), and EpCAM+ cells (epithelial marker on breast tumor cells) were isolated from a minimally (TIL070) and an extensively infiltrated (TIL069) tumor. Expression of select cytokine/chemokine genes analyzed by qRT-PCR (red, high expression/low ΔCt; blue, low expression/high ΔCt; normalized to *SDHA*, *TBP*, and *TMBIM4* as endogens).

immunosuppressive quality of individual BCs varies, with the tendency for SN from tumors sustaining an extensive lymphocyte infiltrate to be less immunosuppressive than those minimally infiltrated (Figure 6, C–I). A direct comparison of gene expression in TIL from extensively versus minimally infiltrated tumors supports this conclusion by showing that extensively infiltrated tumors have greater similarity to S donor cells and minimally infiltrated tumors have greater similarity to SN+S donor cells (Figure 6F and Supplemental Table 6G).

Significance of extensive infiltration. The consistently divergent pattern of gene expression detected in CD4+ TIL from extensively versus minimally infiltrated tumors led us to examine the specific genes affected. These analyses found that a variety of immune response genes are expressed at elevated levels in TIL from extensively infiltrated BC, with many perhaps reflecting their higher level of activation (Figure 7A and Supplemental Table 2G). The most distinctive increase consistently detected in extensively infiltrated tumors was *CXCL13*, with CD4+ TIL shown to be the principal cellular source (Figure 7, B and C). *CXCL13* mRNA expression in tumor sections was recently shown to predict survival of patients with BC, particularly in the HER2+ subtype, although the cell source was not identified (38). An earlier study suggested tumor cells were the major CXCL13 producers in BC but their IHC protocol used higher concentrations of a monoclonal antibody that intensely labeled most cells, both in the tumor tissue and the LN control (39). In contrast, our IHC experiments, using lower concentrations of a polyclonal antibody, stained only some GC-located cells in the LN control, the tumor-associated TLS, and the occasional intratumoral lymphocyte (Supplemental Figure 4C), suggesting that CXCL13 production by tumor cells needs to be reexamined.

In secondary lymphoid organs, such as LNs, CXCL13 is expressed by stromal cells and Th cells in GC, with its ectopic expression promoting lymphoid neogenesis (40). A comparison of *CXCL13* expression with other cytokines/chemokines in an extensively and a minimally infiltrated tumor (Figure 7C) showed that the majority were expressed by infiltrating leukocytes (CD14+ monocytes, CD4+ T cells, or the remaining mixture of CD45+ cells) but not the EpCAM+ epithelial/tumor cells. In general, antitumor cytokines/chemokines were detected at considerably higher levels in the extensively compared with the minimally infiltrated tumors

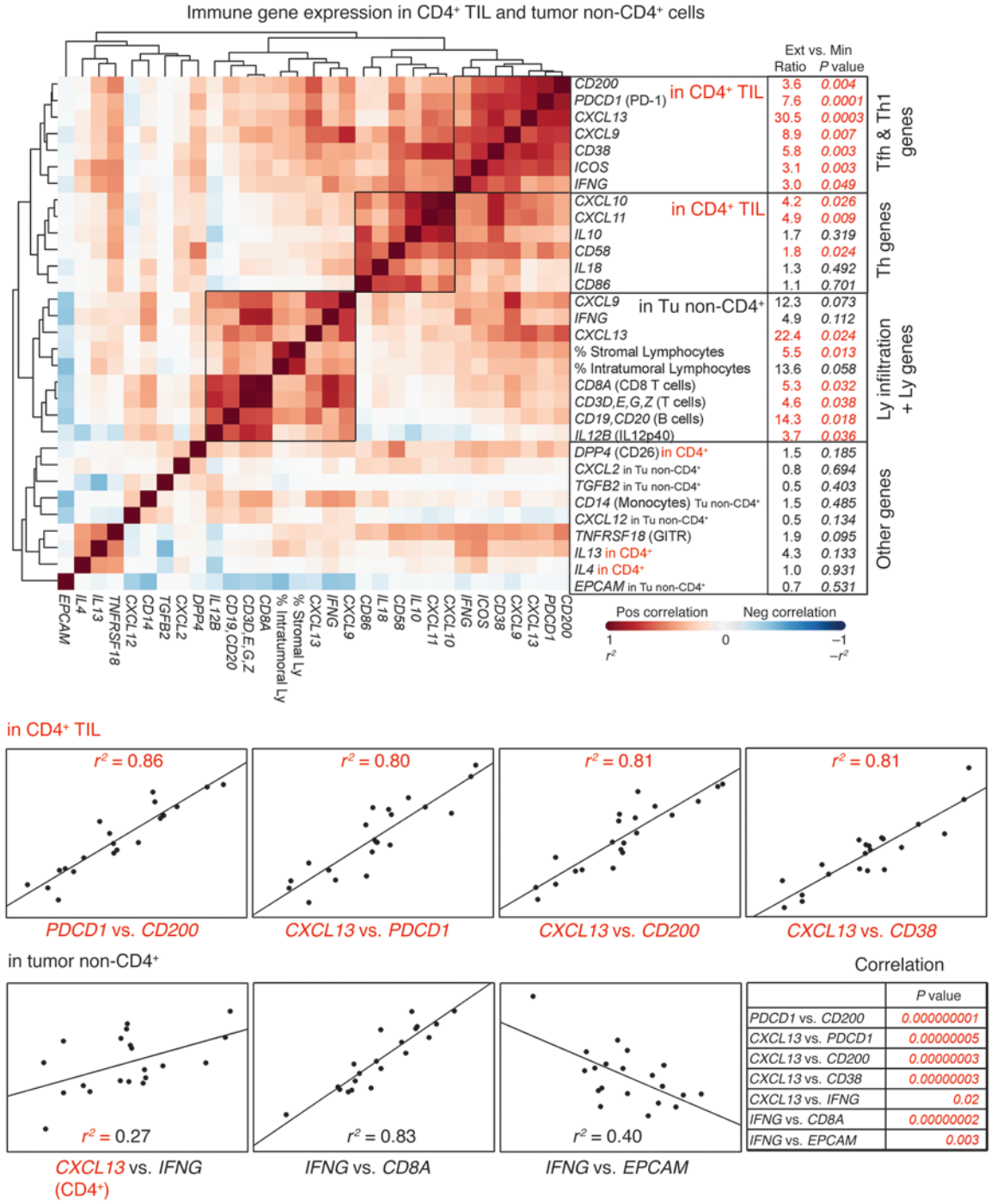

Figure 8

Correlation among the expression of Tfh marker genes, a Th1 immune profile, and the extent of lymphocyte infiltration. qRT-PCR ΔCt values for immune genes expressed in CD4+ TIL (normalized to the Th-specific endogen *CASC3*) or non-CD4 cells (normalized to the 3 endogens in Figure 7C) from 21 tumors were used to generate unsupervised hierarchical clustering. The immune genes include differentially expressed CD4+ TIL surface receptors (Figure 2D) and cytokine/chemokine genes elevated in extensively infiltrated TIL (Figure 3). In the non-CD4 cells, expression of major immune subpopulation markers and cytokines associated with Th1 (*IL12*), Th2 (*IL4* and *IL13*), immune suppression (*IL10* and *TGFB2*), tumor promotion (*CXCL2* and *CXCL12*), and the tumor marker *EPCAM* were analyzed. Pearson correlation coefficients (r^2) were calculated for individual gene combinations or with lymphocyte infiltration levels (Supplemental Table 5D). A negative correlation ($-r^2 = -1$) is shown in blue and a positive correlation ($r^2 = 1$) is shown in red. Fold change (ratio) and *P* values for extensively ($n = 6$) versus minimally ($n = 12$) infiltrated tumors are indicated (significant values are shown in red; $P < 0.05$). Additionally, select correlation plots are shown for relevant surface marker and *CXCL13* gene expression in CD4+ TIL (red) and non-CD4+ cells (black) (significant values are shown in red; $P < 0.05$).

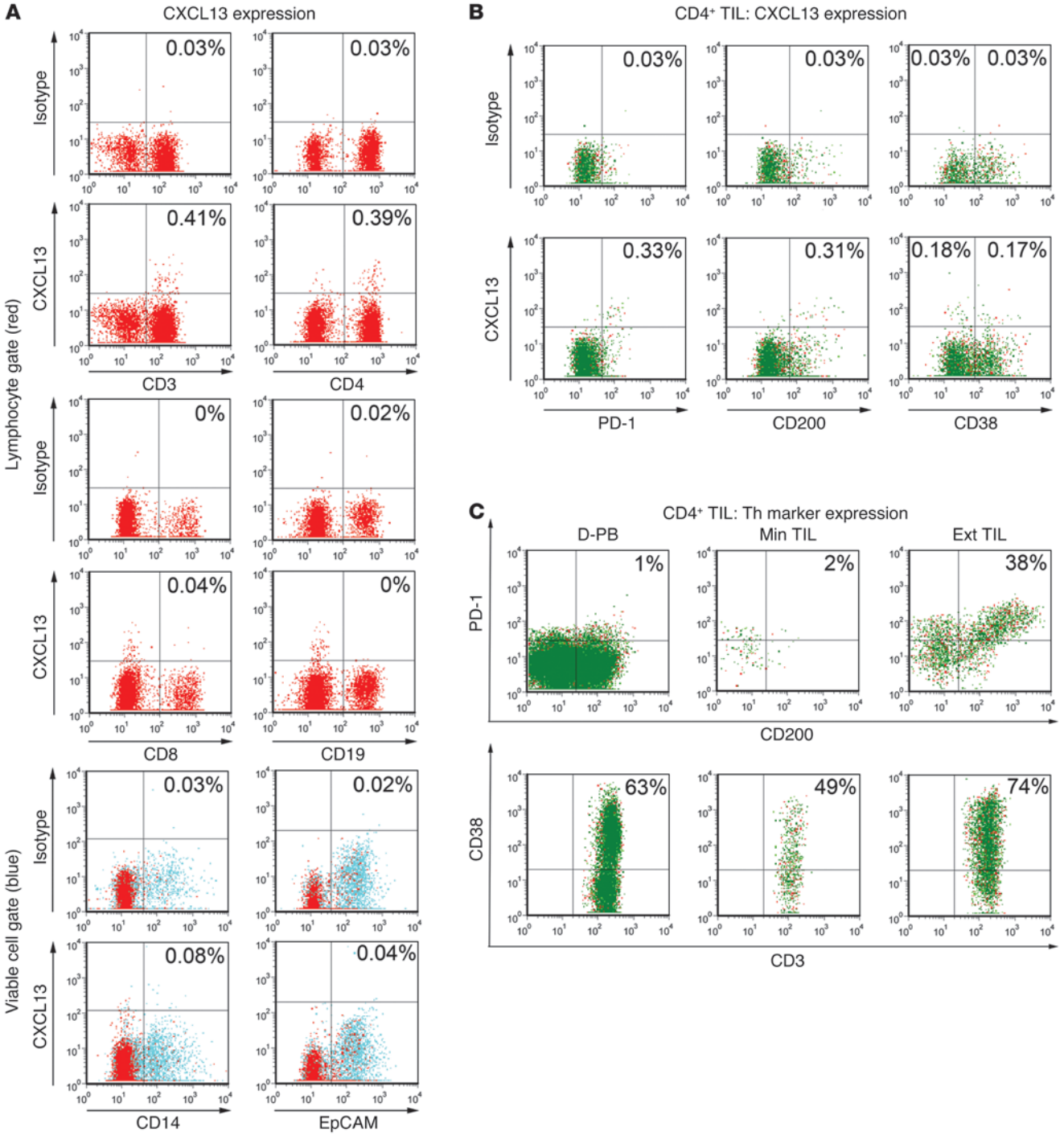

Figure 9

Tfh TIL are the major producers of CXCL13 protein. (**A**) Dot plots of intracellular CXCL13 protein expression in conjunction with subpopulation surface markers (total markers = 17; Supplemental Figure 3) in fresh tumor homogenates (unstimulated). Lymphocyte gate for total T cells (CD3), T cell subsets (CD4 and CD8), and B cells (CD19) or viable cell gate for monocytes (CD14) and epithelial/tumor cells (EpCAM). (**B**) Intracellular CXCL13 expression levels in CD4$^+$ TIL associated with the CD200 and PD-1 (Tfh) or CD38 (Th1). (**C**) Tfh (CD200^{hi} and PD-1^{hi}) and Th1 (CD38^{hi}) surface markers on D-PB and CD4$^+$ TIL from an extensive and a minimally infiltrated tumor.

(except the protumor chemokine *CXCL12*). CD4$^+$ T cells and CD14$^+$ monocytes produced the proinflammatory cytokine IL-18 and IFN-γ–induced chemokines *CXCL9*, *CXCL10*, and *CXCL11*, while *IFNG* itself originated principally from the remaining CD45$^+$ cells (presumably CD8$^+$ T cells; Figure 8 showing a high correlation among *CD8*, *CD3*, and *IFNG* gene expression in the non-CD4$^+$ cells).

To gain a better understanding of the relationship between differences detected consistently in extensively versus minimally infil-

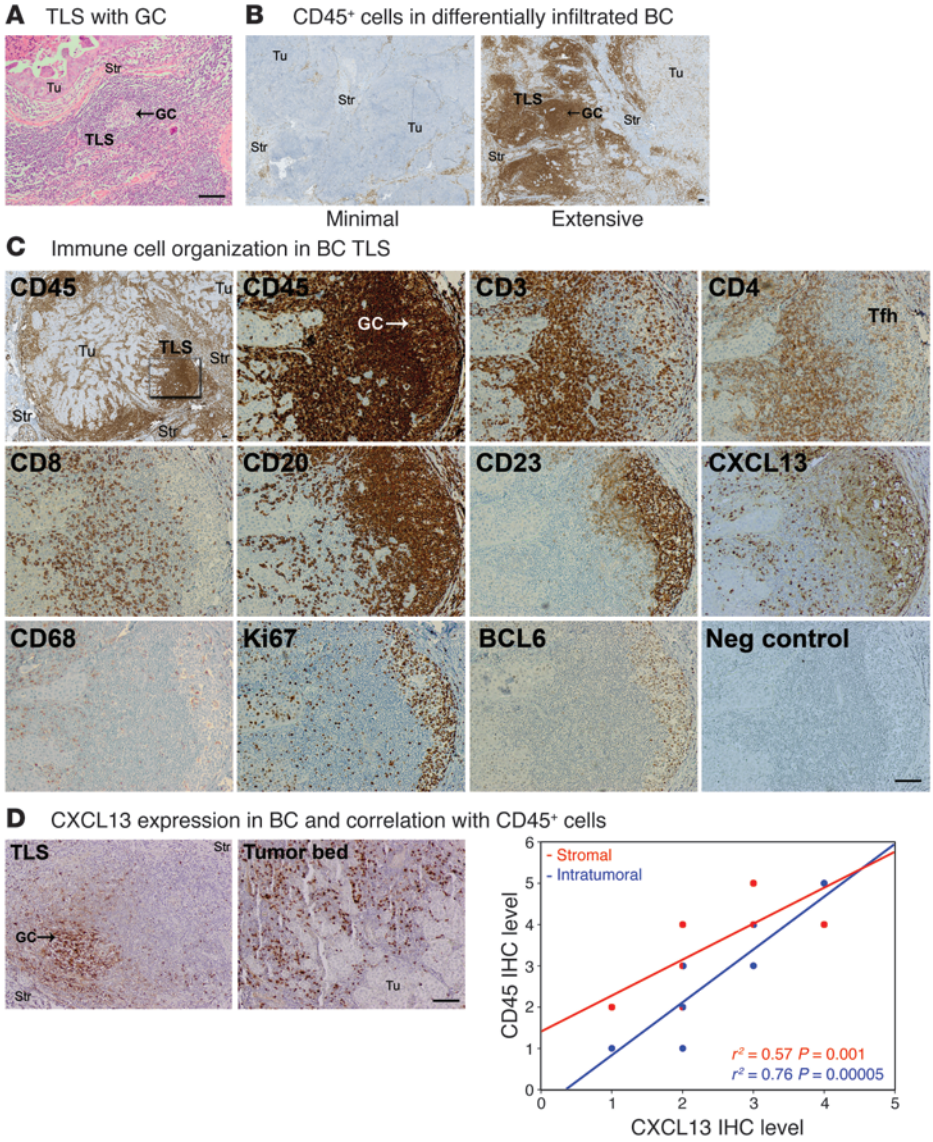

Figure 10
Organization of the immune infiltrate in extensively infiltrated breast tumors. (**A**) TLS containing GC detected in H&E-stained primary tumor sections. Tu, tumor bed; Str, stroma. (**B**) CD45 (total leukocytes) IHC staining of an extensively and a minimally infiltrated tumor shown for comparison. (**C**) Successive paraffin-embedded tumor sections from 15 patients were stained by IHC for CD45 (total leukocytes); CD3 (total T cells); CD4 (helper T cells); CD8 (cytotoxic T cells); CD20 (B cells); CD23 (GC FDCs); CD68 (macrophages); Ki67 (dividing cells; 5 patients); Bcl6 (Tfh and GC B cells; 5 patients); and CXCL13 (Tfh and FDC marker). The boxed area in the first CD45 image is the area magnified in all of the following images of sequential sections labeled with leukocyte subpopulation markers. (**D**) CXCL13 IHC staining in tumor sections (LN control; Supplemental Figure 4) shows cytoplasmic expression in GC-localized cells and some lymphocytes infiltrating the tumor bed (but not in tumor cells). The intensity of CXCL13 staining was correlated with the extent of stromal (red) or intratumoral (blue) $CD45^+$ infiltrates for 15 tumors. Scale bar: 100 μm.

trated tumors and CXCL13 expression levels, we used qRT-PCR data and lymphocyte infiltration intensities from 21 tumors to produce a correlation plot and generate unsupervised hierarchical clustering (Figure 8 and Supplemental Table 5D). This analysis showed that expression of the *IFNG*, *CXCL9*, *CXCL10*, *CXCL11*, and *CXCL13* genes is correlated with *CD38*, *CD58*, *CD200*, *ICOS*, and *PDCD1* gene expression in $CD4^+$ TIL. Furthermore, these genes were also significantly correlated with lymphocyte infiltration and more specifically with $CD8^+$ T cell and B cell marker expression in the non-$CD4^+$ tumor fraction and negatively correlated with the tumor marker *EPCAM*. Expression of the surface receptor genes characteristic for Tfh cells (*CD200* and *PDCD1*) (41) and Th1/activated T cells (*CD38*) (42) correlated best with *CXCL13* gene expression in the $CD4^+$ TIL. This is supported by flow cytometry experiments that showed that CXCL13 is predominantly expressed by T cells (primarily $CD4^+$) but not B cells, other $CD45^+$ cells, $EpCAM^+$ epithelial/tumor cells, or endothelial/stromal cells ($STRO1^+$, $endoglin^+$, $CD10^+$, or $CD271^+$) (Figure 9A and Supplemental Figure 3). Specifically, the principal CXCL13-producing cells were $CD200^{hi}$ $PD\text{-}1^{hi}$ ($CD38^{\pm}$) Tfh cells (Figure 9B). While *CXCL13* expression and that of the Th1 marker, *CD38*, are correlated, this non-Tfh receptor is not specific for CXCL13-producing cells, providing additional support for the concept that Tfh, and not other Th, cells produce CXCL13. These experiments also demonstrate that infiltrates from extensively infiltrated tumors are distinguished by $CD200^{hi}$ $PD\text{-}1^{hi}$ Tfh cells (Figure 9C). Thus, evidence emerged from our analyses that, in the $CD4^+$ fraction, a Tfh profile ($CD200^{hi}$, $PD\text{-}1^{hi}$, ICOS, and *CXCL13*) was associated with a Th1 profile ($CD38^{hi}$, *IFNG*, and *CXCL9*) and both were associated with more extensive lymphocyte infiltration.

CXCL13-producing $CD4^+$ Tfh cells infiltrating breast tumors signal organized immunity. In secondary lymphoid organs, T cells and B cells segregate to separate zones based on CCR7 and CXCR5 expression (28). Upon activation, B cells and $CD4^+$ T cells migrate to the T/B interface for critical interactions that ultimately direct high-affinity $CXCR5^+$ Tfh cells and B cells to migrate in response to CXCL13 to the B cell follicle interior. Once there, they initiate formation of the GC, the site in which memory B cells and long-lived plasma cells

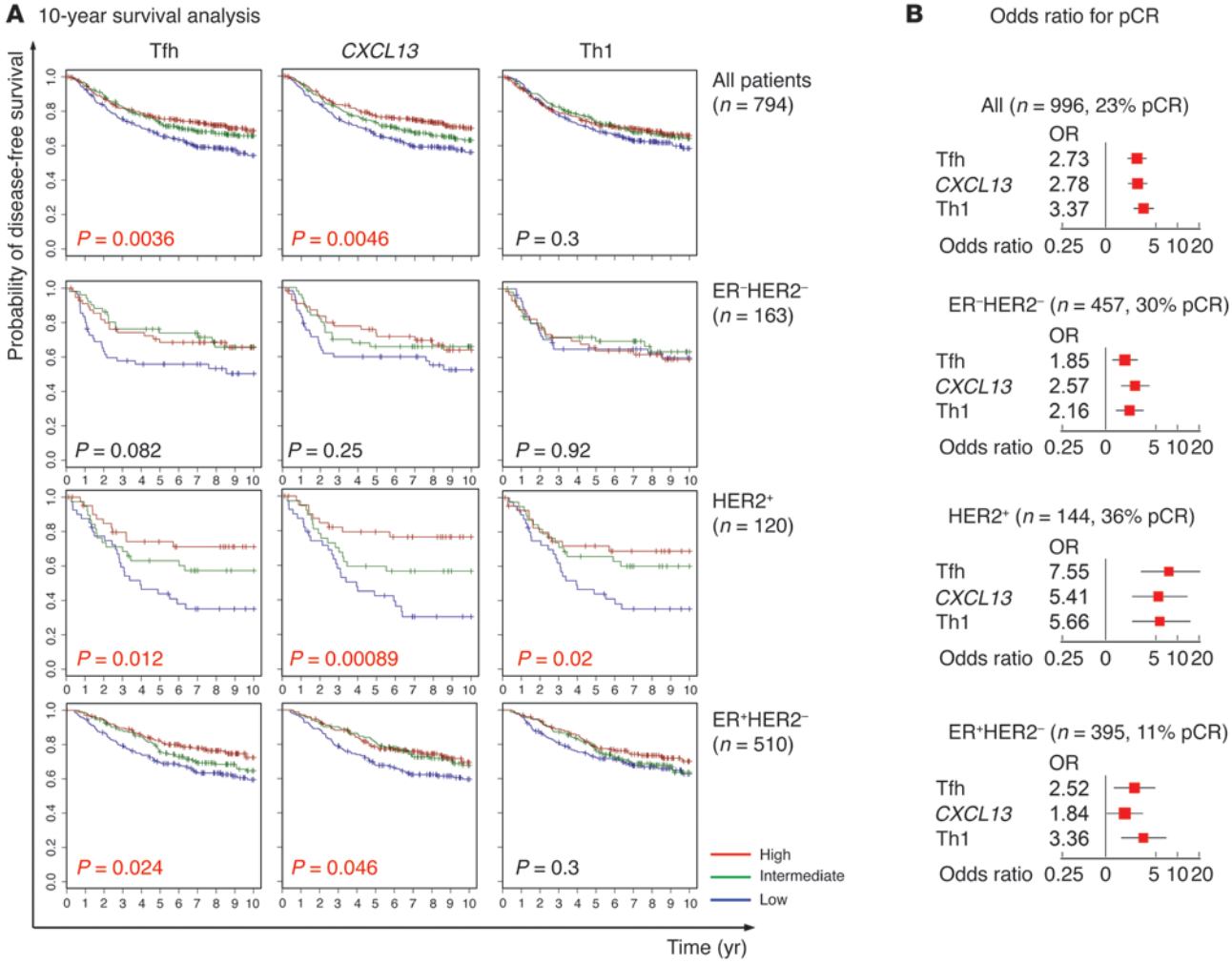

Figure 11

An 8-gene Tfh signature strongly predicts positive clinical outcome in BC. (**A**) Our Tfh (plus *CXCL13* alone) and Th1 signatures were tested on public microarray data sets from 794 primary systemically untreated patients with BC for 10-year DFS (Supplemental Table 7). Kaplan-Meier survival curves were generated for the total patient population and 3 major BC subsets: $ER^-/HER2^-$, $HER2^+$, and $ER^+/HER2^-$; 1 patient was unclassified). Gene expression levels are defined as tertiles of the continuous signature scores: blue, low; green, intermediate; and red, high. *P* values in red are significant ($P < 0.05$). (**B**) Our Tfh (plus *CXCL13* alone) and Th1 signatures were also tested on a group of 966 patients for predicting pCR to neoadjuvant chemotherapy (44). Forest plots show the odds ratios (ORs) for pCR in the total patient population and the indicated subtypes. The size of the square ($P < 0.05$ in red indicates a nominal significant effect) is inversely proportional to the standard error, with the horizontal bars representing the 95% CI of the odds ratio. Signature genes and additional data, including comparisons with published immune signatures, are in Supplemental Table 7.

are generated. Our identification of a Tfh gene expression profile in extensively infiltrated tumors (highlighted by a strong CXCL13 signal) led us to examine BC for lymphoid aggregates and organized TLS containing GC (Figure 10A, Supplemental Figure 4, and Supplemental Table 1C). TLS and GC were detected adjacent to the tumor bed at a higher incidence in extensively compared with minimally infiltrated tumors (Figure 10B and Supplemental Table 1D). The intensity and distribution of the major $CD45^+$ TIL subpopulations within the TLS and GC were analyzed using IHC (Figure 10C and Supplemental Figure 4). BC TLS organization is similar to that of LNs, containing a $CD3^+$ T cell zone adjacent to a $CD20^+$ B cell follicle with $CD23^+$ follicular DCs (FDCs) and $Bcl6^+$ Tfh and GC B cells (43) exclusive to the GC, in which $Ki67^+$ cells (proliferating B cells) are also concentrated. $CD4^+$ T cells are the principal component of the T cell zone and also have a significant presence in the GC. $CD8^+$ T cells were moderately interspersed with $CD4^+$ T cells in the T cell zone but absent from the GC; however, they were the principal lymphocyte population in the tumor bed and present at levels that parallel the extent of the total $CD45^+$ infiltrate and the number/size of TLS (Supplemental Figure 4). CXCL13 was principally expressed by T cell zone or GC lymphocytes (primarily infiltrating $CD4^+PD\text{-}1^{hi}CD200^{hi}$ Tfh cells; Figure 9, A and B) and FDCs, with intratumoral $CXCL13^+$ lymphocytes detected in some extensively infiltrated tumors (Figure 10D). Interestingly, in a very small GC located within a large TLS (Supplemental Figure 4H), we observed $CD4^+$ T cells and CXCL13 protein associated with $CD23^{lo}$ B cells but not $CD23^{hi}$ FDCs, which might signify that CXCL13-producing Tfh cells associate with B

cells earlier than FDCs. Specific CXCL13 labeling of tumor cells was not observed with our IHC conditions (n = 15; Figure 10, C and D, and Supplemental Figure 4), which is consistent with our flow cytometry data (Figure 9A). Furthermore, CXCL13 IHC labeling was correlated with the extent of immune infiltration. CXCL13-producing Tfh cells and FDCs might catalyze the recruitment of other immune cells to the tumor, thereby initiating and/or enhancing TLS development and GC formation. The increased frequency of TLS and GC in conjunction with increased Tfh and Th1 gene expression in CD4$^+$ TIL from extensively infiltrated BC, together with the combined activated/suppressed TIL profile, suggests that immune structures adjacent to the tumor bed may represent an important site for antitumor immune responses.

Clinical significance of CD4$^+$ Tfh cells infiltrating tumors. We tested this hypothesis by investigating the prognostic associations of Th gene expression profiles as a reflection of lymphocyte infiltration levels and/or a TLS presence in a given BC sample. We derived signatures by extracting the most significant and specific Tfh and Th1 genes from the Th subset gene profiles (Figure 1, C and E) that were differentially expressed between extensively and minimally infiltrated tumors (detailed in Supplemental Table 7). We evaluated the association of these signatures with disease-free survival (DFS) in systemically untreated primary BC (n = 794 patients receiving no hormone or chemotherapy before or after surgery; Figure 11A) and compared them with 2 published immune signatures (refs. 6, 8, and Supplemental Table 7). Our Tfh signature (8 genes) was consistently prognostic, demonstrating a linear association with survival in the whole population (P = 0.0036) as well as in the 3 main BC subtypes: HER2$^+$ (P = 0.012), ER$^+$/HER2$^-$ (P = 0.024), with borderline significance observed in ER$^-$/HER2$^-$ (P = 0.082). Given the importance of CXCL13 in Tfh and B cell recruitment, its prognostic associations as a single gene were also investigated, revealing a particularly strong association for the HER2$^+$ subtype, as recently reported (38). The dominant prognostic value of *CXCL13* within the Tfh signature is a reflection of its number one ranking in TIL gene expression changes detected in the extensive versus minimal comparison and our demonstration that Tfh cells are the principal producer cells in BC. This is in contrast to the Treg/activated T cell marker *FOXP3*, which as a single gene did not have any significant predictive value (Supplemental Table 7B). Our Th1 signature (12 genes) predicted survival in the HER2$^+$ BC (P = 0.02) subtype, with the genes *CXCL9* and *IFNG* providing similar results (Supplemental Table 7B).

We next examined a BC cohort treated with preoperative chemotherapy (n = 996) (44), which is given up front prior to surgery with the pathological complete response (pCR) of the tumor (its disappearance at surgery) known to be associated with excellent long-term survival outcome. In this treatment setting, the Tfh and Th1 signatures, along with the *CXCL13* single gene, were all strongly associated with a higher rate of pCR, particularly in the HER2$^+$ subtype (Figure 11B and Supplemental Table 7C). Together, these data support our hypothesis that the presence of CXCL13-producing Tfh cells may specify a TLS/GC presence in the tumor, with these structures producing antitumor immune responses associated with improved clinical responses.

Discussion

The work presented in this study provides new insight into the composition and strategic location of the CD4$^+$ T cell infiltrate and its association with clinical outcome in BC. We identified several aspects of the CD4$^+$ T cell presence that we consider to be fundamentally important. First, while all Th subsets are present in the tumor they do not contribute equally, with more extensively infiltrated tumors distinguished by higher expression of Tfh, Th1, and T cell activation markers. Second, the mixture of activation and suppression observed in the CD4$^+$ TIL (and S+SN–treated donor cells) suggests that their position and prevalence within the tumor dictates responsiveness, with extensively infiltrated tumors successfully sequestering higher concentrations of leukocytes in organized lymphoid structures (TLS). Third, despite tumor-mediated TCR/CD3 pathway suppression, the expression of some key immune transcription factors is consistently upregulated, and a restricted group of cytokines/chemokines are produced by the TIL. Fourth, BCs with extensive immune infiltrates are characterized by the presence of TLS, principally located adjacent to the tumor bed, which house the majority of CXCL13-producing Tfh cells and GC. Fifth, expression of an 8-gene Tfh signature that includes the *CXCL13* gene was associated with a higher likelihood of response to preoperative chemotherapy and better DFS in systemically untreated patients with BC. Together, these data reveal that a detectable Tfh cell presence is associated with organized immune structures and long-term positive clinical outcome.

A recent quantitative evaluation of the leukocyte composition in breast tumors found that CD4$^+$ and CD8$^+$ TIL had an activated (CD27^{lo}CD69^{hi}HLA-DR^{hi}CCR4^{hi}CCR5^{hi}) memory (CD45RA$^-$CCR7$^-$) phenotype (29). Our broad examination of surface markers in conjunction with gene expression profiling confirms and extends these findings by demonstrating that the CD4$^+$ TIL are effector memory cells with all Th subpopulations represented. In contrast to most studies, we found that the CD4$^+$ TIL produce a restricted repertoire of Th cytokines/chemokines, which are generally expressed at sub–T cell activation levels, particularly in minimally infiltrated tumors. The difference between our data and previous work could be attributed to our rapid isolation of CD4$^+$ TIL without in vitro expansion, which provided insight into their in situ state, as well as our inclusion of minimally infiltrated tumors. Finally, eliminating enzymatic digestion, shown to alter TIL function and phenotype (45), also allowed us to retain SN from primary tumor homogenates for treatment of donor CD4$^+$ T cells, which largely reproduced the TIL profiles in activated CD4$^+$ T cells, further validating these data.

Curiously, this reduction in T cell activation and consequent low level cytokine/chemokine expression in the TIL is set against a background of upregulated *REL* and AP-1 superfamily transcription factors. *REL* (c-Rel) is a major player in the canonical NF-κB signaling pathway, integrating T cell activation signals and promoting Th1, Th17, and Treg responses (46). The conserved, homologous E3 ubiquitin ligase proteins, pellino 1 and 2, positively regulate NF-κB activation (47), with c-Rel shown to accumulate in T cells from mice deficient for *PELI1* (48). While a specific function for pellino 2 in T cells has not been reported, it has been shown to regulate NF-κB–dependent IL-8 promoter activity (49). We detected a decrease in *PELI2* in the TIL (Supplemental Table 2B), suggesting a potential mechanism for the observed upregulation of *REL* and *IL8* gene expression.

AP-1/ATF factors also regulate important immune response genes, exemplified by their well-known cooperation with NFAT factors to induce cytokine gene expression (50). We detected upregulation of *JUN*, *FOS* (*FOSB*/*FOSL2*), and *ATF3* in the TIL

and SN+S–treated donor cells in parallel with a decrease in *JUN*, *FOSB*, and *ATF3* in the rested TIL, suggesting that their expression is induced when activated cells enter the tumor microenvironment. A recent study has shown that AP-1 (FOS) is persistently upregulated in infiltrating T cells during tumor progression in mice (51). FOS upregulation specifically induces PD-1 expression on CD4 and CD8 TIL, which mediates their suppression upon contact with PD-L1–expressing tumor cells. While PD-L1 is not expressed on normal breast tissue, studies have shown that it is upregulated in breast tumors, particularly in high proliferative, ER^- BC (52). Disruption of AP-1–induced PD-1 expression on murine TIL was able to restore their cytokine expression (51), with potentially the same mechanism evoked for the reduced cytokine expression we detected in the global $CD4^+$ TIL population. Based on current data, the role(s) PD-1 plays in regulating Tfh cells (a minority of the total $CD4^+$ TIL) remains unclear. Murine studies have shown that $PD\text{-}1^+$ Tfh cell interactions with $PD\text{-}L1^+$/$PD\text{-}L2^+$ B cells are important for regulating GC activities, with a deficiency in PD-L2 resulting in reduced Tfh IL-21 production and the generation of fewer plasma cells (53). The notion that PD-1 expression on Tfh cells elicits context-dependent responses in protected lymphoid structures is supported by a recent murine study showing that $PD\text{-}1^+$ Tfh cells survive and function in gut-associated lymphoid follicles after anti–Thy-1 antibody treatment (54). PD-1 expression is often considered a sign of T cell exhaustion; however, our expanding knowledge indicates that it can also act as a signal for other functions, highlighted by the demonstration that $CD8^+$ $PD\text{-}1^+$ TIL produce higher levels of IFN-γ than $PD\text{-}1^-$ cells (55). Overall, current data suggests that, in contrast to effector T cell TIL, $PD\text{-}1^+$ Tfh cells located in BC-associated TLS likely do not contact $PD\text{-}L1^+$ tumor cells and are not directly affected by PD-1–mediated tumor suppression but are instead regulated by PD-1 to elicit other functions.

Studies of TIL have used various approaches to address the specific influence(s) exerted by individual Th subsets in the tumor microenvironment. Traditionally, Th1-mediated immunity has been considered as antitumoral, because patients whose tumors contain higher levels of Th1 cells are predicted to have longer DFS, while tumors associated with polarized Th2 and/or Treg subpopulation markers have a poorer prognosis (19). This view is complicated by the plasticity of Th differentiation (56), which involves shared surface receptors and cytokines that are often rapidly modulated in time and place, making it frequently difficult to clearly discriminate the type of response(s). Despite these limitations, a number of studies have shown that infiltrating T cell subsets can be used to gauge clinical outcome. The widely studied immune infiltrate in colorectal carcinoma has established that a higher density of intratumoral $CD8^+$ and/or $CD3^+$ memory cells is frequently associated with a better prognosis (57, 58). Tumor-associated Th1 cytokines, lead by IFN-γ, have consistently been linked with more potent antitumor immune responses in a variety of solid tumors (59, 60), with recent research showing that tumor-specific Th1 cells can effectively control tumor development (61, 62). Although IL-17 has been correlated with both protumor and antitumor immune responses (63), Th17 cells have been shown to synergize with IFN-γ to induce the important antitumor chemokines CXCL9 and CXCL10 (64), suggesting that the positive or negative Th17 activities reported may be context dependent. Presence of $Foxp3^+$ Tregs in tumors is also inconsistent among tumor types, with their accumulation in some cancers associated with reduced patient survival, while in others they signal a better outcome. An important early study by Curiel et al. (65) found that tumor-associated Tregs were correlated with suppressed antitumor immunity and reduced survival in ovarian carcinoma. Foxp3 expression by tumor cells was shown to be an independent predictor of improved outcome in patients with $HER2^+$ BC (66). A recent study of colorectal cancer has found that the presence of $Foxp3^+$ tumor cells ($Epcam^+$) but not $Foxp3^+$ $CD4^+$ T cells is indicative of a poor prognosis (67). In BC, the majority of studies investigating $CD4^+$ TIL have been focused on Tregs (68), with their increased presence linked with a poor prognosis in ER^+ disease (21, 69) but a good clinical outcome in ER^- disease (70). Further investigation is needed to more clearly define the roles played by individual Th subpopulations in different types of BC.

In this study, we have extended current knowledge of Th subsets infiltrating solid tumors by showing that, in addition to Th1 cells, a measurable Tfh presence is also significant and associated with better BC patient outcome. Tfh cells are relative newcomers to the Th subset family (71, 72) and have not been previously described in nonhematological tumors. While their role in antitumor immunity is unknown, studies of cellular interactions in secondary lymphoid organs show that Tfh cells are key players in the generation of T cell–dependent antibody responses and B cell memory (73). Collectively, these data (predominantly from animal models) demonstrate that these specialized Th cells are intimately involved in GC development and provide critical help for antigen-specific B cell maturation to high-affinity memory cells and long-lived plasma cells (28, 43, 74). While long considered minor players in antitumor immunity (75), plasma cells infiltrating non–small cell lung cancer (76) and $CD20^+$ B cells infiltrating BC (77), ovarian cancer (78), melanoma (79), and colorectal carcinoma (80) have been associated with increased survival. Studies of B cells in BC have detected specific antibody responses to tumor antigens (81, 82) and correlated B cell gene expression signatures with better clinical outcome (9, 83). The data presented here show that the most important differences in the TIL profiles were related to the extent of infiltration, which identified important Th subset differences characterized by increased Th1 and particularly Tfh marker expression in extensively infiltrated tumors. We found that a detectable Tfh presence predicts longer survival in untreated patients as well as pCRs in preoperatively treated patients, which further suggests that B cell responses may constitute an important component of effective antitumor immunity in BC. Although the role(s) B cells play in cancer immunity is currently undefined, they could potentially affect antitumor immune responses via their antibody-producing capacities, APC functions, and/or production of specific cytokines and chemokines.

We found that a Tfh presence was principally associated with peritumoral TLS, which have been described primarily in the lung, in patients with chronic inflammatory diseases or as a reactive response to infection (84). These organized structures contain distinct T cell zones and B cell follicles with reactive GC similar to secondary lymphoid organs. Some earlier studies described lymphoid aggregates or organized lymphoid structures in tumors, including BC (81); however, their prognostic value has only recently been investigated in a study of non–small cell lung cancer, in which the number of mature DCs was used as an indicator for TLS (26), and in colorectal cancer, in which both lymphocyte aggregates (57) and active TLS, the latter identified

by high chemokine expression levels (27), were associated with a better clinical outcome. While lymphoid structures containing FDCs or a high density of endothelial venules have been described in BC (81, 85) and other tumors, their immunological importance in these patients has not been specifically addressed. Our analysis of $CD4^+$ T cell subsets in BC TLS found that elevated levels of CXCL13 expression were correlated with Tfh markers and the extent of tumor infiltration. These data led us to further demonstrate that CXCL13-producing Tfh cells signal the presence of organized TLS containing reactive GC that are associated with favorable clinical outcomes. Studies have shown that CXCL13 (in conjunction with CCL19, CCL21, TNF, and lymphotoxin) plays a critical role in the development and maintenance of secondary lymphoid organs (86) and is essential for dynamic GC formation in response to acute infection. Although CXCL13 has principally been defined as a stromal cell–produced (including FDCs) chemokine, PD-1^{hi} Th cells were recently shown to be efficient CXCL13 producers (87). Our experiments used a variety of approaches to demonstrate that $CD4^+$PD-$1^{hi}$$CD200^{hi}$ Tfh cells infiltrating BC are a major source of CXCL13 production.

In BC, a high immune signal has been linked with better progression-free survival in overall patient groups as well as aggressive BC subtypes, including $HER2^+$ (7, 8, 10), ER^-/$HER2^-$ (8, 10, 11), and highly proliferative tumors (9). The signals emanating from these analyses of total tumor tissue detect a broad spectrum of immune response genes, reflecting activities of the innate and adaptive immune responses, with some refined to a T cell metagene (10), B cell metagene (9), or signaling pathways (8). Additionally, two recent studies demonstrated that a higher immune score in the initial biopsy predicts increased pCR rates after preoperative chemotherapy (88), with the strongest association observed in the $HER2^+$ and ER^-/$HER2^-$ subtypes (44). Generally, higher expression of an immune signature reflects a greater presence of immune cells, with the latter associated with a better prognosis. Our data confirm and extend these findings by demonstrating that a key positive prognostic element detected by these immune signatures is a Tfh presence in organized TLS, which may be a surrogate for effective responses to the tumor. A link between the patient's natural ability to mount what appears to be a more comprehensive immune response in LN-like structures adjacent to the tumor bed and clinical outcome suggests that some patients might derive specific benefit from therapies designed to boost their immunity before the tumor, as a source of antigen, is removed.

The major findings in this study indicate that, despite the immune system's failure to contain the growing tumor, the presence of CXCL13-producing Tfh cells is associated with organized immune structures adjacent to the tumor bed that potentially participate in propagating sustainable and effective long-term antitumor immunity. Leukocytes within the TLS could thus dynamically respond to evolving local tumor antigens, maintain activation, and generate long-lived memory cells while sequestered in a protected microenvironment. The mixture of activation and suppression that we observed in the $CD4^+$ TIL may reflect the presence of functionally activated cells from the TLS combined with suppressed cells migrating through the intratumoral and peritumoral regions. Despite their imminent suppression once they move from the TLS, we suggest that some tumor-specific memory cells survive and maintain effective immunosurveillance that functions over the long-term to detect and eliminate residual tumor cells. Thus, patients whose immune systems mount an organized response to their tumors, specifically detectable by the Tfh signature, would be predicted to have a better response to preoperative chemotherapy or postsurgical DFS.

Methods

Patient population and clinical samples. Tumor, LN, and/or blood samples were obtained from 70 untreated patients undergoing tumor resection for BC at the Jules Bordet Institute. Fresh tumor tissue, LN tissue, and PB from the 10 patients in the discovery set (P1–P10) and fresh tumor tissue from 60 patients in the confirmation set (TIL003–TIL132; and ipsilateral nonadjacent normal breast tissue when available) were analyzed. PB samples from 19 healthy female adults were used as controls for the discovery set (D1–D4) and the confirmation set (D5–D19). Clinicopathological patient data is detailed in Supplemental Table 1.

Tumor sample preparation. Dissected tumor fragments from fresh surgical specimens were directly transferred into 3 ml X-VIVO 20 (Lonza) before 2 rapid rounds of mechanical dissociation with the GentleMACS Dissociator (Program A.01; Miltenyi Biotec). This approach yielded a >50% increase in cell viability compared with enzymatic digestion. The resulting cell suspension was filtered following each dissociator run using a 40-μm cell strainer (BD Falcon), washed with X-VIVO 20, centrifuged for 15 minutes at 600 *g*, and resuspended in X-VIVO 20 before isolation or flow cytometric analysis. The tumor SN was the initial 3 ml of X-VIVO 20 recovered after the first round of dissociation, which was subsequently clarified by centrifugation for 15 minutes at 13,000 *g*.

Cell isolation. For molecular analyses, $CD4^+$ T cells were positively purified from patient samples or healthy donor blood using Dynabeads CD4 (Invitrogen). Memory $CD4^+$ T cells were purified by CD45RA depletion (Dynabeads M450 Epoxy [Invitrogen] coupled to an anti-CD45RA antibody [304102; Biolegend]) prior to $CD4^+$ selection. Additional tumor cell populations were purified using Dynabeads M-450 Epoxy coupled with monoclonal antibodies to CD14, CD45, or EpCAM (301801, 304001, and 324201; Biolegend). For primary cells treated with tumor SN, total $CD4^+$ or memory ($CD45RA^-$ = RO^+) $CD4^+$ cells were negatively purified using the $CD4^+$ T cell Isolation Kit II or Memory $CD4^+$ T cell Isolation Kit (Miltenyi Biotec). The cell purification protocols were controlled by flow cytometry with negatively purified samples >98% pure and positively isolated $CD4^+$ TIL >95% pure.

Treatment with tumor SN. Total $CD4^+$ or memory $CD4^+$ cells (2×10^6 cells/ml) purified from healthy donor blood were incubated in X-VIVO 20 overnight following isolation. Cell viability was controlled the following day by flow cytometry (>95%), and then an equal volume of tumor SN or X-VIVO 20 was added with or without anti-CD3 (317304, clone OKT3; Biolegend) and anti-CD28 (555725, clone CD28.2; BD Pharmingen), each at 1 μg/ml final concentration. The cells were recovered 24 hours after treatment for analysis using microarrays, qRT-PCR (including a kinetic experiment for *IFNG* and *IL2* gene expression over 48 hours after treatment; Supplemental Table 5H), and/or flow cytometry.

Microarrays. 10 ng (discovery set) or 100 ng (confirmation set) high-quality total RNA was labeled following the manufacturer's protocols for probe preparation and hybridization on the Affymetrix U133 Plus 2.0 GeneChip. The gene expression array data has been deposited into the Gene Expression Omnibus under accession number (GSE36769).

Flow cytometry. Samples assessed for the expression of 60 cell surface markers (duplicates or triplicates were assessed for each marker) were incubated individually or in combinations of antibodies (listed in Supplemental Figures 1–3) for 45 minutes at 4°C in 50 μl X-VIVO 20 followed by washing with 2 ml PBS and immediate analysis on a FACSCalibur (BD Biosciences) without fixation. The Cytofix/Cytoperm Kit (BD Biosciences) was used for intracellular staining with anti-CXCL13 (IC801A; R&D Systems).

qRT-PCR. RNA was extracted using TRIzol Reagent (Invitrogen) and reverse transcribed into cDNA using the High-Capacity RNA-to-cDNA Kit (Applied Biosystems) following standard procedures. Real-time PCR reactions were performed using commercially available Gene Expression Assays (Applied Biosystems or Qiagen) or published primers (detailed in Supplemental Table 5A) and iTaq SYBR Green Supermix With ROX (Bio-Rad) on an ABI 7900HT Prism sequence detector (Applied Biosystems).

Immunohistochemistry. Four-μm sections of paraffin-embedded tumor blocks from P1–P10 were labeled with anti-CD4 and anti-CD3 antibodies. Successive sections from 15 patients from the confirmation set were labeled with the top 9 antibodies listed in Supplemental Figure 4 using the Endogenous Biotin Blocking Kit (Ventana) and iVIEW DAB Detection Kit (Ventana) on a BenchMark XT IHC/ISH slide stainer (Ventana). For CXCL13 labeling, mounted sections were deparaffinized with xylene, pretreated with citrate 10 mM, pH 6.0, at 95°C to 99°C for 20 minutes, exposed to a 3% hydrogen peroxide solution to quench endogenous peroxidase activity, and blocked with rabbit serum (Sigma-Aldrich) for 1 hour prior to incubation with a purified goat anti-human polyclonal antibody to CXCL13 (1:100, AF801; R&D Systems) in a moist chamber at 4°C overnight. For each tumor, one section was treated in parallel without the primary antibody as a negative control. Subsequent incubations were carried out with a biotinylated rabbit anti-goat secondary antibody (Vector Laboratories) for 30 minutes at room temperature, followed by the HRP streptavidin reagent (Zymed) and the DAB + Substrate Chromogen System (Dako). The slides were counterstained with hematoxylin (Sigma-Aldrich) and mounted on a Tissue-Tek Prisma Automated Slide Stainer (Sakura).

Survival analysis. The Th1 and Tfh gene signatures derived in this study along with previously published immune gene signatures were assessed for their power to predict either 10-year DFS or pCR after neoadjuvant chemotherapy. DFS analyses were performed using 794 systemically untreated patients with BC from 8 public microarray data sets (Supplemental Table 7F). The signature scores (signed average of expression values for the genes in the signature) were computed as in Desmedt et al. (8). Three categories of gene expression cut-off values (high, intermediate, and low) were defined using tertiles of the continuous signature scores. In these data sets, BC subtypes were defined using a 2-gene classification based on *ESR1* (also known as ER) and *ERBB2* (also known as HER2) gene expression (89). pCR analyses were performed using 966 patients treated with neoadjuvant chemotherapy from 8 published studies, as in Ignatiadis et al. (44). BC subtypes were defined on the basis of ER protein expression by IHC and HER2 amplification by IHC and fluorescent in situ hybridization in the original publications. When unavailable, ER and HER2 status was assigned according to bimodal normalized *ESR1* and *ERBB2* gene expression (44). The association between an individual gene signature and pCR was based on an estimated odds ratios and 95% CI (44).

Statistics. *P* values for nonmicroarray data were generated using a 2-tailed Student's *t* test with unequal variance (or a χ^2 test where indicated). A *P* value of less than 0.05 was considered as significant. Individual patient microarray data, our experimental data, and publicly available data for individual Th subsets were differentially analyzed based on the type and number of samples in the set by using the specifically adapted methods and criteria detailed in Supplemental Methods.

Study approval. All primary breast tissue, LN, and blood samples used in this study were taken from individuals treated at the Institute Jules Bordet. All patients signed a protocol-specific consent. Healthy donor blood samples were taken from volunteers who signed an informed consent. The protocols used for human studies were approved by the Medical Ethics Committee of the Institut Jules Bordet.

Acknowledgments

We thank Nicolas Sirtaine for advice in reading the H&E slides, Samira Majjaj for technical advice on the gene chip hybridizations, and Anne Zerghe and Ghizlane Rouas for expert technical assistance in establishing the tumor homogenate protocols and CXCL13 IHC experiments, respectively. This work was supported by grants from the Belgian Fund for Scientific Research (FNRS), Les Amis de l'Institut Bordet, FNRS-Opération Télévie, Plan Cancer of Belgium, Fonds Lambeau-Marteaux, and Fonds Barsy. C. Gu-Trantien is a fellow and S. Garaud is a postdoc at the FNRS-Télévie, and C. Sotiriou is a research director at the FRS-FNRS.

Received for publication December 19, 2012, and accepted in revised form April 25, 2013.

Address correspondence to: Karen Willard-Gallo, Molecular Immunology Unit, Institut Jules Bordet, Université Libre de Bruxelles, 121 Blvd. de Waterloo, B1000 Brussels, Belgium. Phone: 32.2.541.3739; Fax: 32.2.541.7325; E-mail: kwillard@ulb.ac.be.

Sherene Loi's present address is: Peter MacCallum Cancer Centre, East Melbourne, Victoria, Australia.

Marie Ravoet's present address is: Centre de Génétique Humaine, Cliniques Universitaires St. Luc-UCL, Bruxelles, Belgium.

Benjamin Haibe-Kains's present address is: Bioinformatics and Computational Genomics Laboratory, Institut de recherches cliniques de Montréal, Montreal, Quebec, Canada.

Stefan Michiels's present address is: Service de Biostatistique et d'Epidémiologie, Institut Gustave-Roussy, Villejuif, France.

1. Perou CM, et al. Molecular portraits of human breast tumours. *Nature*. 2000;406(6797):747–752.
2. Sorlie T, et al. Gene expression patterns of breast carcinomas distinguish tumor subclasses with clinical implications. *Proc Natl Acad Sci U S A*. 2001; 98(19):10869–10874.
3. Sotiriou C, Pusztai L. Gene-expression signatures in breast cancer. *N Engl J Med*. 2009;360(8):790–800.
4. Sotiriou C, et al. Gene expression profiling in breast cancer: understanding the molecular basis of histologic grade to improve prognosis. *J Natl Cancer Inst*. 2006;98(4):262–272.
5. Ascierto ML, et al. An immunologic portrait of cancer. *J Transl Med*. 2011;9:146.
6. Teschendorff AE, Miremadi A, Pinder SE, Ellis IO, Caldas C. An immune response gene expression module identifies a good prognosis subtype in estrogen receptor negative breast cancer. *Genome Biol*. 2007;8(8):R157.
7. Alexe G, et al. High expression of lymphocyte-associated genes in node-negative HER2+ breast cancers correlates with lower recurrence rates. *Cancer Res*. 2007;67(22):10669–10676.
8. Desmedt C, et al. Biological processes associated with breast cancer clinical outcome depend on the molecular subtypes. *Clin Cancer Res*. 2008; 14(16):5158–5165.
9. Schmidt M, et al. The humoral immune system has a key prognostic impact in node-negative breast cancer. *Cancer Res*. 2008;68(13):5405–5413.
10. Rody A, et al. T-cell metagene predicts a favorable prognosis in estrogen receptor-negative and HER2-positive breast cancers. *Breast Cancer Res*. 2009;11(2):R15.
11. Yau C, Esserman L, Moore DH, Waldman F, Sninsky J, Benz CC. A multigene predictor of metastatic outcome in early stage hormone receptor-negative and triple-negative breast cancer. *Breast Cancer Res*. 2010;12(5):R85.
12. Ascierto ML, et al. A signature of immune function genes associated with recurrence-free survival in breast cancer patients. *Breast Cancer Res Treat*. 2012; 131(3):871–880.
13. Rody A, et al. A clinically relevant gene signature in triple negative and basal-like breast cancer. *Breast Cancer Res*. 2011;13(5):R97.
14. Rahir G, Moser M. Tumor microenvironment and lymphocyte infiltration. *Cancer Immunol Immunother*. 2012;61(6):751–759.
15. Mahmoud SM, et al. Tumor-infiltrating CD8+ lymphocytes predict clinical outcome in breast cancer.

J Clin Oncol. 2011;29(15):1949–1955.
16. Mahmoud S, Lee A, Ellis I, Green A. CD8(+) T lymphocytes infiltrating breast cancer: A promising new prognostic marker? *Oncoimmunology*. 2012; 1(3):364–365.
17. Bos R, Marquardt KL, Cheung J, Sherman LA. Functional differences between low- and high-affinity CD8(+) T cells in the tumor environment. *Oncoimmunology*. 2012;1(8):1239–1247.
18. Bos R, Sherman LA. CD4+ T-cell help in the tumor milieu is required for recruitment and cytolytic function of CD8+ T lymphocytes. *Cancer Res*. 2010; 70(21):8368–8377.
19. Ruffell B, DeNardo DG, Affara NI, Coussens LM. Lymphocytes in cancer development: polarization towards pro-tumor immunity. *Cytokine Growth Factor Rev*. 2010;21(1):3–10.
20. Zamarron BF, Chen W. Dual roles of immune cells and their factors in cancer development and progression. *Int J Biol Sci*. 2011;7(5):651–658.
21. Gobert M, et al. Regulatory T cells recruited through CCL22/CCR4 are selectively activated in lymphoid infiltrates surrounding primary breast tumors and lead to an adverse clinical outcome. *Cancer Res*. 2009;69(5):2000–2009.
22. Wilke CM, et al. Th17 cells in cancer: help or hindrance? *Carcinogenesis*. 2011;32(5):643–649.
23. Ye J, Livergood RS, Peng G. The role and regulation of human Th17 cells in tumor immunity. *Am J Pathol*. 2013;182(1):10–20.
24. deLeeuw RJ, Kost SE, Kakal JA, Nelson BH. The prognostic value of FoxP3+ tumor-infiltrating lymphocytes in cancer: a critical review of the literature. *Clin Cancer Res*. 2012;18(11):3022–3029.
25. de Chaisemartin L, et al. Characterization of chemokines and adhesion molecules associated with T cell presence in tertiary lymphoid structures in human lung cancer. *Cancer Res*. 2011;71(20):6391–6399.
26. Dieu-Nosjean MC, et al. Long-term survival for patients with non-small-cell lung cancer with intratumoral lymphoid structures. *J Clin Oncol*. 2008; 26(27):4410–4417.
27. Coppola D, et al. Unique ectopic lymph node-like structures present in human primary colorectal carcinoma are identified by immune gene array profiling. *Am J Pathol*. 2011;179(1):37–45.
28. Vinuesa CG, Cyster JG. How T cells earn the follicular rite of passage. *Immunity*. 2011;35(5):671–680.
29. Ruffell B, Au A, Rugo HS, Esserman LJ, Hwang ES, Coussens LM. Leukocyte composition of human breast cancer. *Proc Natl Acad Sci U S A*. 2012; 109(8):2796–2801.
30. Chtanova T, et al. Identification of T cell-restricted genes, and signatures for different T cell responses, using a comprehensive collection of microarray datasets. *J Immunol*. 2005;175(12):7837–7847.
31. Miyara M, et al. Functional delineation and differentiation dynamics of human CD4+ T cells expressing the FoxP3 transcription factor. *Immunity*. 2009;30(6):899–911.
32. Lee MS, Hanspers K, Barker CS, Korn AP, McCune JM. Gene expression profiles during human CD4+ T cell differentiation. *Int Immunol*. 2004; 16(8):1109–1124.
33. Ravoet M, et al. Molecular profiling of CD3-CD4+ T cells from patients with the lymphocytic variant of hypereosinophilic syndrome reveals targeting of growth control pathways. *Blood*. 2009; 114(14):2969–2983.
34. Zaunders JJ, et al. Early proliferation of CCR5(+) CD38(+++) antigen-specific CD4(+) Th1 effector cells during primary HIV-1 infection. *Blood*. 2005; 106(5):1660–1667.
35. Baniyash M. TCR zeta-chain downregulation: curtailing an excessive inflammatory immune response. *Nat Rev Immunol*. 2004;4(9):675–687.
36. Fazilleau N, Mark L, McHeyzer-Williams LJ, McHeyzer-Williams MG. Follicular helper T cells: lineage and location. *Immunity*. 2009;30(3):324–335.
37. Balkwill FR. The chemokine system and cancer. *J Pathol*. 2012;226(2):148–157.
38. Razis E, et al. Improved outcome of high-risk early HER2 positive breast cancer with high CXCL13-CXCR5 messenger RNA expression. *Clin Breast Cancer*. 2012;12(3):183–193.
39. Panse J, et al. Chemokine CXCL13 is overexpressed in the tumour tissue and in the peripheral blood of breast cancer patients. *Br J Cancer*. 2008;99(6):930–938.
40. Link A, et al. Association of T-zone reticular networks and conduits with ectopic lymphoid tissues in mice and humans. *Am J Pathol*. 2011; 178(4):1662–1675.
41. Crotty S. Follicular helper CD4 T cells (TFH). *Annu Rev Immunol*. 2011;29:621–663.
42. Viegas MS, et al. CD38 plays a role in effective containment of mycobacteria within granulomata and polarization of Th1 immune responses against Mycobacterium avium. *Microbes Infect*. 2007; 9(7):847–854.
43. Crotty S. The 1-1-1 fallacy. *Immunol Rev*. 2012; 247(1):133–142.
44. Ignatiadis M, et al. Gene modules and response to neoadjuvant chemotherapy in breast cancer subtypes: a pooled analysis. *J Clin Oncol*. 2012; 30(16):1996–2004.
45. Grange C, et al. Phenotypic characterization and functional analysis of human tumor immune infiltration after mechanical and enzymatic disaggregation. *J Immunol Methods*. 2011;372(1–2):119–126.
46. Hayden MS, Ghosh S. NF-kappaB, the first quarter-century: remarkable progress and outstanding questions. *Genes Dev*. 2012;26(3):203–234.
47. Kim TW, et al. Pellino 2 is critical for Toll-like receptor/interleukin-1 receptor (TLR/IL-1R)-mediated post-transcriptional control. *J Biol Chem*. 2012; 287(30):25686–25695.
48. Chang M, et al. The ubiquitin ligase Peli1 negatively regulates T cell activation and prevents autoimmunity. *Nat Immunol*. 2011;12(10):1002–1009.
49. Yu KY, Kwon HJ, Norman DA, Vig E, Goebl MG, Harrington MA. Cutting edge: mouse pellino-2 modulates IL-1 and lipopolysaccharide signaling. *J Immunol*. 2002;169(8):4075–4078.
50. Macian F, Lopez-Rodriguez C, Rao A. Partners in transcription: NFAT and AP-1. *Oncogene*. 2001; 20(19):2476–2489.
51. Xiao G, Deng A, Liu H, Ge G, Liu X. Activator protein 1 suppresses antitumor T-cell function via the induction of programmed death 1. *Proc Natl Acad Sci U S A*. 2012;109(38):15419–15424.
52. Ghebeh H, et al. Expression of B7-H1 in breast cancer patients is strongly associated with high proliferative Ki-67-expressing tumor cells. *Int J Cancer*. 2007;121(4):751–758.
53. Good-Jacobson KL, Szumilas CG, Chen L, Sharpe AH, Tomayko MM, Shlomchik MJ. PD-1 regulates germinal center B cell survival and the formation and affinity of long-lived plasma cells. *Nat Immunol*. 2010;11(6):535–542.
54. Mihalj M, Kellermayer Z, Balogh P. Follicles in gut-associated lymphoid tissues create preferential survival niches for follicular Th cells escaping Thy-1-specific depletion in mice [published online ahead of print February 28, 2013]. *Int Immunol*. doi:10.1093/intimm/dxt001.
55. Inozume T, et al. Selection of CD8+PD-1+ lymphocytes in fresh human melanomas enriches for tumor-reactive T cells. *J Immunother*. 2010; 33(9):956–964.
56. O'Shea JJ, Paul WE. Mechanisms underlying lineage commitment and plasticity of helper CD4+ T cells. *Science*. 2010;327(5969):1098–1102.
57. Galon J, et al. Type, density, and location of immune cells within human colorectal tumors predict clinical outcome. *Science*. 2006;313(5795):1960–1964.
58. Yoon HH, Orrock JM, Foster NR, Sargent DJ, Smyrk TC, Sinicrope FA. Prognostic impact of FoxP3+ regulatory T cells in relation to CD8+ T lymphocyte density in human colon carcinomas. *PloS One*. 2012;7(8):e42274.
59. Shankaran V, et al. IFNgamma and lymphocytes prevent primary tumour development and shape tumour immunogenicity. *Nature*. 2001; 410(6832):1107–1111.
60. Curtis NJ, Primrose JN, Thomas GJ, Mirnezami AH, Ottensmeier CH. The adaptive immune response to colorectal cancer: from the laboratory to clinical practice. *Eur J Surg Oncol*. 2012;38(10):889–896.
61. Haabeth OA, et al. Inflammation driven by tumour-specific Th1 cells protects against B-cell cancer. *Nat Commun*. 2011;2:240.
62. Braumuller H, et al. T-helper-1-cell cytokines drive cancer into senescence. *Nature*. 2013; 494(7437):361–365.
63. Ji Y, Zhang W. Th17 cells: positive or negative role in tumor? *Cancer Immunol Immunother*. 2010; 59(7):979–987.
64. Kryczek I, et al. Phenotype, distribution, generation, and functional and clinical relevance of Th17 cells in the human tumor environments. *Blood*. 2009; 114(6):1141–1149.
65. Curiel TJ, et al. Specific recruitment of regulatory T cells in ovarian carcinoma fosters immune privilege and predicts reduced survival. *Nat Med*. 2004; 10(9):942–949.
66. Ladoire S, et al. Presence of Foxp3 expression in tumor cells predicts better survival in HER2-overexpressing breast cancer patients treated with neoadjuvant chemotherapy. *Breast Cancer Res Treat*. 2011; 125(1):65–72.
67. Kim M, et al. Expression of foxp3 in colorectal cancer but not in treg cells correlates with disease progression in patients with colorectal cancer. *PloS One*. 2013;8(1):e53630.
68. Watanabe MA, Oda JM, Amarante MK, Cesar Voltarelli J. Regulatory T cells and breast cancer: implications for immunopathogenesis. *Cancer Metastasis Rev*. 2010;29(4):569–579.
69. Bates GJ, et al. Quantification of regulatory T cells enables the identification of high-risk breast cancer patients and those at risk of late relapse. *J Clin Oncol*. 2006;24(34):5373–5380.
70. West NR, et al. Tumour-infiltrating FOXP3(+) lymphocytes are associated with cytotoxic immune responses and good clinical outcome in oestrogen receptor-negative breast cancer. *Br J Cancer*. 2013; 108(1):155–162.
71. Breitfeld D, et al. Follicular B helper T cells express CXC chemokine receptor 5, localize to B cell follicles, and support immunoglobulin production. *J Exp Med*. 2000;192(11):1545–1552.
72. Schaerli P, Willimann K, Lang AB, Lipp M, Loetscher P, Moser B. CXC chemokine receptor 5 expression defines follicular homing T cells with B cell helper function. *J Exp Med*. 2000; 192(11):1553–1562.
73. McHeyzer-Williams M, Okitsu S, Wang N, McHeyzer-Williams L. Molecular programming of B cell memory. *Nat Rev Immunol*. 2012;12(1):24–34.
74. Ramiscal RR, Vinuesa CG. T-cell subsets in the germinal center. *Immunol Rev*. 2013;252(1):146–155.
75. Nelson BH. CD20+ B cells: the other tumor-infiltrating lymphocytes. *J Immunol*. 2010;185(9):4977–4982.
76. Lohr M, et al. The prognostic relevance of tumour-infiltrating plasma cells and immunoglobulin kappa C indicates an important role of the humoral immune response in non-small cell lung cancer. *Cancer Lett*. 2013;333(2):222–228.
77. Mahmoud SM, Lee AH, Paish EC, Macmillan RD, Ellis IO, Green AR. The prognostic significance of B lymphocytes in invasive carcinoma of the breast. *Breast Cancer Res Treat*. 2012;132(2):545–553.
78. Nielsen JS, et al. CD20+ tumor-infiltrating lympho-

cytes have an atypical CD27- memory phenotype and together with CD8+ T cells promote favorable prognosis in ovarian cancer. *Clin Cancer Res*. 2012; 18(12):3281–3292.
79. Ladanyi A, et al. Prognostic impact of B-cell density in cutaneous melanoma. *Cancer Immunol Immunother*. 2011;60(12):1729–1738.
80. Maletzki C, Jahnke A, Ostwald C, Klar E, Prall F, Linnebacher M. Ex-vivo clonally expanded B lymphocytes infiltrating colorectal carcinoma are of mature immunophenotype and produce functional IgG. *PLoS One*. 2012;7(2):e32639.
81. Coronella JA, et al. Antigen-driven oligoclonal expansion of tumor-infiltrating B cells in infiltrating ductal carcinoma of the breast. *J Immunol*. 2002; 169(4):1829–1836.
82. Coronella-Wood JA, Hersh EM. Naturally occurring B-cell responses to breast cancer. *Cancer Immunol Immunother*. 2003;52(12):715–738.
83. Bianchini G, et al. Molecular anatomy of breast cancer stroma and its prognostic value in estrogen receptor-positive and -negative cancers. *J Clin Oncol*. 2010;28(28):4316–4323.
84. Foo SY, Phipps S. Regulation of inducible BALT formation and contribution to immunity and pathology. *Mucosal Immunol*. 2010;3(6):537–544.
85. Martinet L, et al. Human solid tumors contain high endothelial venules: association with T- and B-lymphocyte infiltration and favorable prognosis in breast cancer. *Cancer Res*. 2011;71(17):5678–5687.
86. Muller G, Hopken UE, Lipp M. The impact of CCR7 and CXCR5 on lymphoid organ development and systemic immunity. *Immunol Rev*. 2003; 195:117–135.
87. Wang C, Hillsamer P, Kim CH. Phenotype, effector function, and tissue localization of PD-1-expressing human follicular helper T cell subsets. *BMC Immunol*. 2011;12:53.
88. Denkert C, et al. Tumor-associated lymphocytes as an independent predictor of response to neoadjuvant chemotherapy in breast cancer. *J Clin Oncol*. 2010;28(1):105–113.
89. Haibe-Kains B, et al. A three-gene model to robustly identify breast cancer molecular subtypes. *J Natl Cancer Inst*. 2012;104(4):311–325.